energies

MDPI

Article

Stochastic Wake Modelling Based on POD Analysis

David Bastine [1,2], Lukas Vollmer [1,2], Matthias Wächter [1,*] and Joachim Peinke [1,2]

1 AG TWiSt, Institute of Physics, ForWind, University of Oldenburg, Küpkersweg 70, 26129 Oldenburg, Germany; david.bastine@uni-oldenburg.de (D.B.); lukas.vollmer@iwes.fraunhofer.de (L.V.); joachim.peinke@uni-oldenburg.de (J.P.)

2 Fraunhofer Institute for Wind Energy Systems IWES, Am Seedeich 45, 27572 Bremerhaven, Germany

* Correspondence: matthias.waechter@uni-oldenburg.de; Tel.: +49-441-798-5051

Received: 19 January 2018; Accepted: 26 February 2018; Published: 9 March 2018

Abstract: In this work, large eddy simulation data is analysed to investigate a new stochastic modeling approach for the wake of a wind turbine. The data is generated by the large eddy simulation (LES) model PALM combined with an actuator disk with rotation representing the turbine. After applying a proper orthogonal decomposition (POD), three different stochastic models for the weighting coefficients of the POD modes are deduced resulting in three different wake models. Their performance is investigated mainly on the basis of aeroelastic simulations of a wind turbine in the wake. Three different load cases and their statistical characteristics are compared for the original LES, truncated PODs and the stochastic wake models including different numbers of POD modes. It is shown that approximately six POD modes are enough to capture the load dynamics on large temporal scales. Modeling the weighting coefficients as independent stochastic processes leads to similar load characteristics as in the case of the truncated POD. To complete this simplified wake description, we show evidence that the small-scale dynamics can be captured by adding to our model a homogeneous turbulent field. In this way, we present a procedure to derive stochastic wake models from costly computational fluid dynamics (CFD) calculations or elaborated experimental investigations. These numerically efficient models provide the added value of possible long-term studies. Depending on the aspects of interest, different minimalized models may be obtained.

Keywords: wake model; POD; stochastic process; coherent structures; loads; wind turbine; wind turbine loads

1. Introduction

More and more wind turbines are organized in large wind farms containing up to hundreds of turbines. Consequently, a large number of these turbines frequently operates in the wake of other turbines. The reduced wind speed and enhanced turbulence in the wake flow leads to power losses [1,2] and increased fatigue loadings [3]. Therefore, modeling of wakes plays a key role in the design process of wind turbines and entire wind farms [4–7] as well as in the emerging field of wind farm control [8–12].

Wake modeling through fully resolved simulations based on the Navier-Stokes equations is computationally very expensive due to the many scales relevant to turbulent flows [13]. The most detailed dynamical simulations which can be computed in reasonable times are large eddy simulations (LES) [14] combined with simplified turbine models, such as actuator disk or actuator line models [15–24]. Even though these simulations have proven to be an efficient tool for the investigation of specific research questions, LES are still too time-consuming for most practical applications. In particular, long-term studies cannot be performed with such demanding computational fluid dynamics (CFD) tools. Therefore, much simpler wake models are needed, which strongly reduce the computational costs.

A variety of wake models exist which only describe the steady mean velocity deficit in the wake flow. They range from simple kinematic models [25,26] over approximated versions of the Reynolds averaged Navier-Stokes (RANS) equations to combinations of the full RANS equations with simplified turbine models [7]. While these steady models can be used for estimations of the power output, the loads acting on turbines in the wake cannot be calculated from the mean velocity deficit since they strongly depend on the dynamics of the wake flow.

In industry applications the wake dynamics are often taken into account by modeling the additional turbulence intensity caused by the presence of the wake [3,27]. Such a single quantity, however, can obviously not describe all relevant dynamical features of a wake flow. One possible approach to a more precise description is given by the dynamic wake meandering model (DWM) [28–31]. It consists of three major elements, namely a model for a steady velocity deficit, a model describing large-scale movement of the wake caused by large atmospheric structures and a model for the added turbulence caused by the rotor.

The DWM shows some promising results (e.g., [32]), but it remains an open question which features of the wake flow have to be taken into account. In particular, the influence and interplay of different large-scale effects has not yet been understood. For example, laboratory [33] and field measurements [34] indicate that the turbine modulates the atmospheric flow on a wide range of scales, even on scales up to five or more rotor diameters [33].

Another dynamic approach, also followed in this work, is to analyse and model wind turbine wakes using modal decompositions [21,35–47] which describe the velocity field as a linear superposition of spatial modes with time-dependent weighting coefficients. It has been shown that a few spatial modes can already capture important features of the wake flow [35–39,41,43,47]. In the case of a large eddy simulation of an infinite row of turbines, Andersen et al. [35] found that a few modes stemming from the proper orthogonal decomposition (POD) already yield a good description of the velocity field on large spatial scales. For PIV data obtained in a wind turbine boundary layer array, Hamilton et al. [39] have shown that a few modes can approximately reproduce the spatial dependence of the Reynolds stress tensor. In Bastine et al. [38], dynamical features of quantities relevant for a sequential turbine in the wake, such as the energy flux through a disk, could be captured well with only three modes.

Most of the works on decompositions mentioned above only deal with reduced descriptions of the wake while approaches to model the temporal evolution have rarely been investigated. The temporal dynamics of reduced order systems stemming from modal decompositions are completely described by the weighting coefficients of the selected modes [48]. For relatively simple fluid flows, a system of corresponding differential equations can be obtained by projecting the Navier-Stokes Equation on selected POD modes [48,49], which is called a Galerkin projection. For the wind turbine wake, this projection is difficult to handle due to the complex interaction of the flow and the wind turbine. Furthermore, the description and inclusion of a turbulent atmospheric inflow is a very challenging task. An alternative approach, investigated by Iungo et al. [41], Debnath et al. [43], is to linearize the temporal evolution leading to the dynamic mode decomposition [50–53]. In this framework, the relevant weighting coefficients are all periodic. Iungo et al. [41] extended this approach by embedding the reduced system within a Kalman-filter making data-driven modeling possible. Andersen [54] and Andersen et al. [35] found dominant frequency peaks for the weighting coefficients of POD modes extracted from an LES of an infinite row of turbines. They tried to model the coefficients by using only the discovered periodic parts.

In far and intermediate wake regions of a single wake with a turbulent inflow, dominating periodic oscillations are not necessarily present, as indicated by e.g., Singh et al. [33] and Iungo et al. [55]. Hence, this work suggests a new approach modeling the weighting coefficients of a POD as a stochastic process yielding a stochastic wake model. We show that the the temporal dynamics of truncated PODs can be described well by very simple stochastic processes. Furthermore, we investigate the problem of missing turbulent kinetic energy in the modeled wake flow, which is a principle shortcoming of reduced order

models based on modal decompositions. Inspired by similar approaches in [28–31,39], we illustrate that it is possible to capture the small-scale properties of the flow by adding a homogeneous turbulent field to the wake structure, which is modeled by the POD-based approach.

These approaches are investigated through the analysis of an LES of an actuator disk with rotation [56] in a turbulent atmospheric boundary layer (ABL). The obtained POD modes are combined with simple stochastic models for the weighting coefficients. Since we are mainly interested in the impact of the wake flow on sequential turbines, aeroelastic simulations of a wind turbine in the wake are performed. Original LES, truncated PODs and stochastic models are used as inflows and the results are compared for different numbers of modes included.

The article is structured as follows. The LES used in this work is described in Section 2. Subsequently in Section 3, we introduce the methods necessary to obtain the stochastic wake models from the LES data. Furthermore, we illustrate how the performance of the different wake descriptions is investigated based on aeroelastic simulations. The analysis of the LES data begins in Section 4 with a standard POD analysis followed by an investigation of the performance of truncated PODs depending on the number of included modes. Subsequently in Section 5, we deduce the three different stochastic wake models based on the LES data and compare their performance to truncated PODs and the original LES. To mimic the small-scale wake turbulence we add an additional homogeneous turbulent field to one of the stochastic wake models in Section 6 and analyse the performance of this extended model. Conclusions from our results are drawn in Section 7.

2. LES Simulations

The large eddy simulations have been performed using the **PA**rallelized **L**ES **M**odel PALM [57,58], which has been extensively used for the simulation of the atmospheric boundary layer for the last 15 years. PALM solves the non-hydrostatic, incompressible Navier-Stokes Equations under the Boussinesq Approximation using central differences on a uniformly spaced Cartesian staggered grid. For the time integration a third-order Runge-Kutta scheme and for the advection terms a fifth-order Wicker-Skamarock scheme is used. Subgrid-scale turbulence is filtered implicitly and is parametrized by a modified Smagorinsky approach following Deardorff [59].

Recently, PALM has been combined with simplified wind turbine models for the investigation of wind turbine wakes and the simulation of entire wind farms [22,23,56,60]. Here, an enhanced actuator disk model with rotation (ADM-R) is used, which provides close results to an actuator line model in the far wake while being much less computationally expensive [56,61]. The ADM-R parameters are set to model the NREL 5 MW research turbine [62] with a hub height of $z_h = 90\,\mathrm{m}$ and a rotor diameter of $\mathrm{D} = 126\,\mathrm{m}$. Adaptation of the rotor speed to the fluctuating wind speed is ensured by a variable-speed generator-torque controller [62].

The flow field for the simulation with the wind turbine model is established in a pre-run with cyclic boundary conditions that is initialized with a laminar wind profile and is run for 18 hof simulation time until it has reached a quasi-steady state. The development of turbulence is initiated by random perturbations at the beginning of the pre-run. The simulations are run with a roughness length of $z_0 = 2 \cdot 10^{-3}\,\mathrm{m}$, representative for a moderately rough sea surface, a neutral potential temperature profile capped by an inversion at 500 m and a Coriolis parameter for $\phi_{lat} = 54^\circ\,\mathrm{N}$. A uniform grid size of 5 m is chosen with 1024 grid points in along-stream and 512 grid points in cross-stream direction. The time step used for the integration is $dt = 0.3\,\mathrm{s}$ and the analysed data includes 23,500 snapshots corresponding to 7050 s. These numbers are chosen based on former results in [38] and are a compromise between statistical convergence and numerical effort. A short comment on statistical convergence can also be found at the end of Section 4.1.

A turbulent recycling method [58] is used for the simulation with the wind turbine to enable a simulation of a single turbine instead of simulating an infinite row. For this purpose, the domain size is doubled along the along-stream axis. The recycling surface is placed at the domain length

of the precursor run. Undisturbed outflow at the downstream boundary is ensured by a radiation boundary condition.

The mean velocity field far upstream of the turbine is shown in Figure 1a. As all following figures showing yz-planes in the flow domain, the field is plotted from the perspective of an downstream observer looking upstream. The corresponding mean profile can be found in Figure 2a. At hub height the average velocity is approx. 8 $\frac{\mathrm{m}}{\mathrm{s}}$, with a turbulence intensity of approx. 5%. In the following sections, we analyse the stream-wise component u of the wake flow in the yz-plane 3.5 D away from the turbine. Snapshots of this plane are shown in Figure 3. These snapshots nicely illustrate different shapes of the wake structure, which are likely to play an important role for the loads acting on a wind turbine in the wake. As mentioned in the introduction, this is one of the major motivations for investigating a POD-based modeling approach, which can roughly describe different shapes of the wake. The mean velocity at hub height is approx. 4 $\frac{\mathrm{m}}{\mathrm{s}}$, as can be seen in the mean velocity field shown in Figure 1b and the corresponding profile in Figure 2b. The variance at hub height is approximately 0.5 $\mathrm{m}^2\mathrm{s}^{-2}$ resulting in an approximate turbulence intensity of 18%. In the outer region of the wake a strongly increased variance of the field is observed (Figures 1c and 2c).

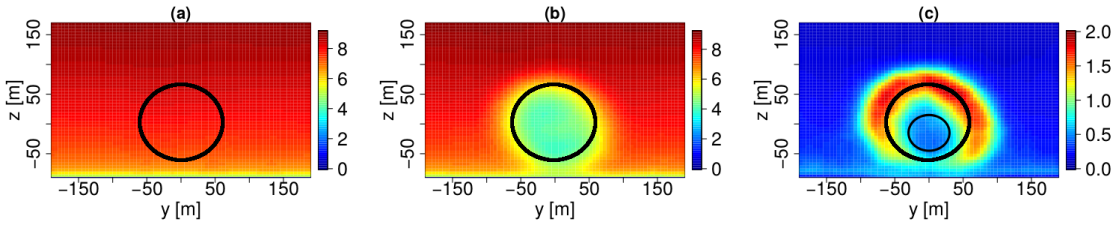

Figure 1. Statistics of the stream-wise velocity $u(y,z,t)$: (**a**) Mean field (ms^{-1}) far upstream of the turbine; (**b**) Mean field (ms^{-1}), 3.5 D away from the turbine; (**c**) Variance $(\mathrm{m}^2\mathrm{s}^{-2})$ 3.5 D away from the turbine. The large black circle marks the rotor area of a turbine in the wake flow, which is modeled later using aeroelastic simulations. The small black circle marks the central region of the wake, which is used to build a spectral surrogate in Section 6.

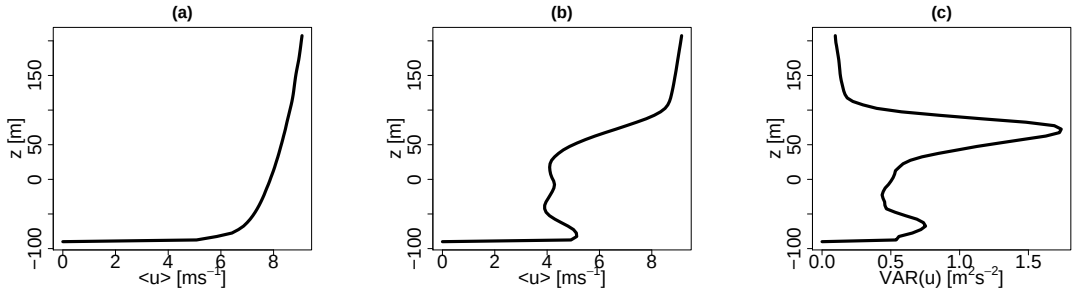

Figure 2. Different profiles at $y = 0$ m corresponding to the figures in Figure 1: (**a**) Mean field far upstream of the turbine; (**b**) Mean field 3.5 D away from the turbine; (**c**) Variance 3.5 D away from the turbine.

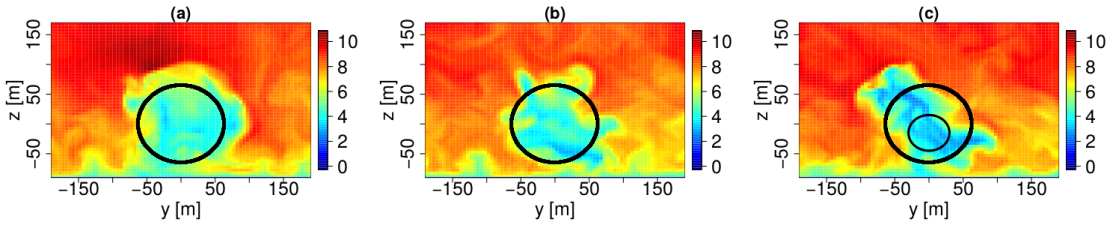

Figure 3. Snapshots of the LES showing the the stream-wise velocity u (ms^{-1}) in a yz-plane 3.5 D away from the turbine. (**a**) $t = 990$ s; (**b**) $t = 1185$ s; (**c**) $t = 1230$ s. The large black circle marks the rotor area of a turbine in the wake flow, which is modeled later using aeroelastic simulations. The small black circle marks the central region of the wake, which is used to build a spectral surrogate in Section 6.

3. Methods

In this work, a stochastic wake modeling approach is developed to capture the dynamics of a wind turbine wake in a new manner. The steps involved in this approach are illustrated on the left hand side of Figure 4. After some basic preprocessing the POD is applied to the LES data resulting in wake descriptions of reduced order. The accuracy of these truncated PODs depends on the number of included POD modes. Afterwards, the weighting coefficients of the POD modes are modeled stochastically instead of using the exact projections on the corresponding POD modes. The accuracy of the resulting stochastic wake models now additionally depends on the complexity of the used stochastic processes. In a last step, a stochastic homogeneous turbulent field based on the original LES simulations is added to the stochastic wake models.

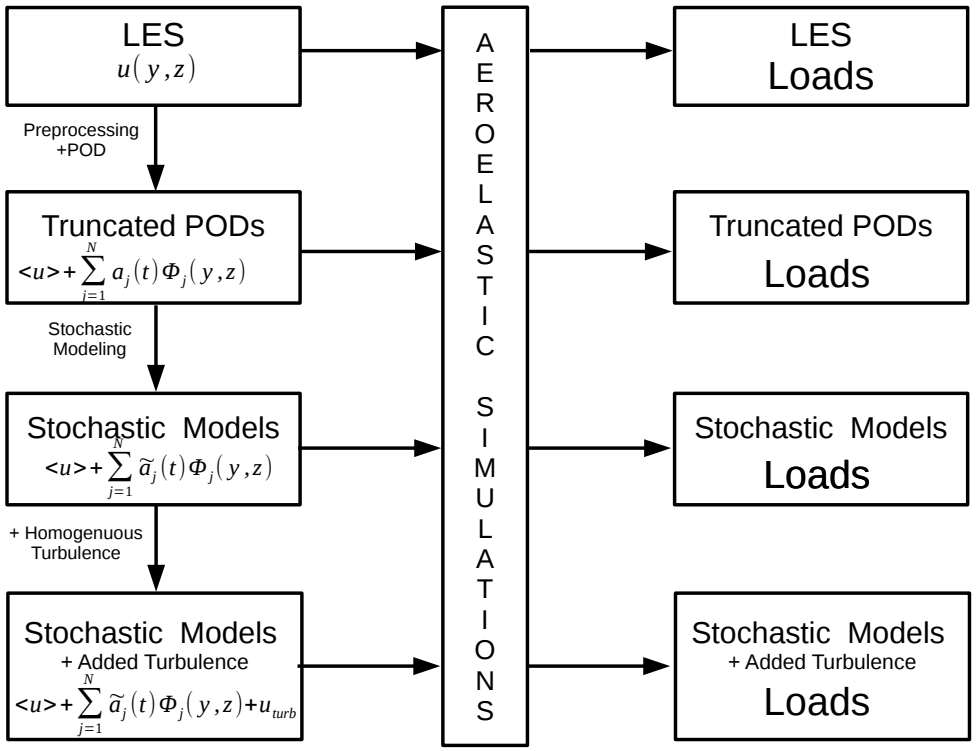

Figure 4. Illustration of our modeling approach and its verification: In the left part of the figure, the different steps leading to reduced wake descriptions are presented. These different descriptions are all used as inflows to aeroelastic simulations. All resulting loads are then compared in order to give insight into the strength and weaknesses of the simplified wake flows. The mathematical notation used in the figure will be explained in the rest of this section.

Several assumptions and simplifications are made in our procedure, which in the end have to be justified by a satisfactory performance of the resulting models. Thus, in addition to comparing the direct properties of the resulting velocity fields, we use these fields as inflows to a wind turbine using aeroelastic simulations, as also indicated by Figure 4. We then compare the resulting loads of the original LES and the different wake descriptions in order to draw conclusions on their performance and the necessary complexity of stochastic wake models.

In the following, we will now explain the different steps involved in our modeling approach and its verification in greater detail.

3.1. Preprocessing

Before the POD is applied to the data, the velocity field is preprocessed similarly as in Bastine et al. [38] to focus the analysis on the wake structure. Coherent structures which are only

weakly influenced by the wake should be excluded from the analysis. The preprocessing is illustrated in Figure 5. First, we subtract the mean field far upstream of the turbine (Figure 1a) from the wake flow (Figure 5a). The resulting velocity deficit obtained after additionally changing the sign of the field is shown in Figure 5b. Second, we extract the deficit by using a relative threshold for every time step. This means that we set all values smaller than a certain threshold of the current deficit maximum to zero. In our case, the value 40% worked very well. This extraction is followed by a dilation procedure [63] to keep the neighbouring regions which are lower than the threshold but still belong to the wake structure. The kernel used for the dilation is a disk with radius 20 m. The resulting extracted deficit is shown in Figure 5c.

It should be noted that the stochastic modelling approach presented in the following does not qualitatively rely on the chosen preprocessing procedure. Changing parameters, such as the threshold value, only leads to minor quantitative differences. Even when the analysis was performed confined to a fixed circular region around the wake centre, instead of using a threshold, qualitatively similar results were obtained. The threshold procedure is chosen, since in our former work [38] it lead to a smaller number of necessary POD modes than the approach with the fixed region.

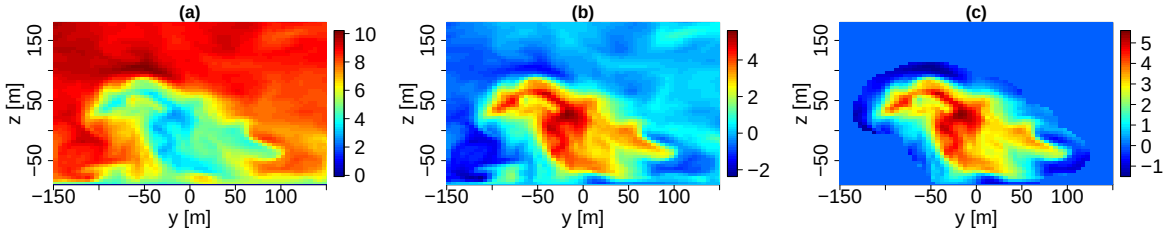

Figure 5. Preprocessing of the velocity field u (ms^{-1}) : (**a**) Instant Snapshot $t = 31.8$ s; (**b**) Velocity deficit; (**c**) Extracted deficit.

3.2. POD

A decomposition of the velocity field $u(y,z,t)$ into spatial modes with time-dependent weighting coefficients can be written as:

$$u(y,z,t) = \langle u(y,z,t)\rangle_t + \sum_{j=1}^{\infty} a_j(t)\phi_j(y,z)\,, \tag{1}$$

where $\langle \ldots \rangle_t$ denotes averaging over time. In case of the POD, the $\phi_j(y,z)$ are called POD modes, which can be defined as the eigenfunctions of the covariance operator solving:

$$\int dy'dz'\ \langle u'(y,z,t)u'(y',z',t)\rangle_t\ \phi_j(y',z') = \lambda_j\phi_j(y,z) \tag{2}$$

with $u' = u - \langle u\rangle_t$. The covariance operator is a compact self-adjoint operator yielding a countable number of real eigenvalues, which are usually ordered as $\lambda_1 > \lambda_2 > \ldots$ The corresponding orthogonal POD modes $\phi_j(y,z)$ can also be chosen as real-valued functions with corresponding weighting coefficients $a_j(t)$ obtained through the projection:

$$a_j(t) = (\phi_j|u') := \int dy'dz'\ \phi_j(y',z')u'(y,z,t)\,. \tag{3}$$

It should be noted that in case of performing the POD on simulation data on a spatial grid, as done here, Equation (2) is commonly approximated by the eigenvalue problem of the discretized covariance matrix $C_{ij} = \langle u_i'(t)u_j'(t)\rangle_t$. where $u(y,z)$ is substituted by u_k as the value of u at the k-th grid point.

When aiming for a reduced description of the velocity field it is common practice to truncate the POD after N modes yielding:

$$u^{(N)}(y,z,t) := \langle u(y,z,t)\rangle_t + \sum_{j=1}^{N} a_j(t)\phi_j(y,z)) \approx u(y,z,t). \tag{4}$$

For such approximations of the field u, the POD modes solving Equation (2) are the optimal modes with respect to the turbulent kinetic energy. More precisely, they are the set of orthogonal modes with the smallest mean squared error [48] given by

$$\langle \|u'(y,z,t) - \sum_{j=1}^{N} a_j(t)\phi_j(y,z)\|_2^2\rangle_t \text{ , with } a_j(t) = (\phi_j|u') \text{ .} \tag{5}$$

Another important property of the POD is that the temporal behaviour of the weighting coefficients is uncorrelated:

$$\langle a_i(t)a_j(t)\rangle_t = \lambda_i\delta_{ij} \text{ ,} \tag{6}$$

which simply comes from the fact that the covariance operator is diagonal in the basis of its own eigenvectors.

Using Equation (4) the POD offers a systematic, and in an energetic sense, optimal way to reduce the complexity of the velocity field. The number of modes N needed to obtain a useful approximation of the flow is often much lower than the number of grid points. This leads to a strong dimensional reduction of the system. In the case of a wind turbine wake in the yz-plane, a typical grid point number is in the order of 10^3–10^4 with approximately 40 modes needed to capture 80% of the turbulent kinetic energy, as for example discussed in Andersen [54] and Bastine et al. [38] and also found in Section 4.1 for our case of 3250 grid points. In this work, we often aim at a reduction to a system with 10 or less modes, which will be referred to as using only "a few" modes in the following.

3.3. Temporal Stochastic Modelling

Although the POD can lead to a reduced description of the field, no modelling of the temporal dynamics is involved. A truncated POD, as given by Equation (4), can simply be viewed as a special kind of spatially filtered field. Nonetheless, the POD naturally suggests an approach for the description of the temporal dynamics, since all dynamical information lies in the weighting coefficients $(a_j(t))_{i=1}^N$ of the N selected modes. Therefore, in this paper we aim for an efficient way to model the time-dependence of these weighting coefficients. Our Ansatz is to describe these N weighting coefficients $(a_j(t))_{j=1}^N$ as a stochastic system. In this article, we additionally assume that the weighting coefficients are statistically independent yielding a description of the $(a_j(t))_{j=1}^N$ by N one-dimensional stochastic processes. It should be noted, that even though the assumption of independence is inspired by Equation (6), it obviously leads to a significant approximation since the non-linear coupling of different scales in the fluid dynamical equations is neglected. It therefore has to be justified by a satisfactory performance of the deduced model.

In the following, $\tilde{a}_j(t)$ denotes the stochastic process (or a corresponding realisation) which models the j-th weighting coefficient. The symbol $a_j(t)$ denotes the time series stemming from the projection of the original LES on the j-th POD mode (Equation (3)). Inserting $\tilde{a}_j(t)$ instead of $a_j(t)$ into a truncated POD (Equation (4)) leads to the corresponding stochastic wake model given by

$$\tilde{u}^{(N)}(y,z,t) = \langle u(y,z,t)\rangle_t + \sum_{j=1}^{N} \tilde{a}_j(t)\phi_j(y,z) \text{ .} \tag{7}$$

Three different ways to model the weighting coefficients will be introduced in the following resulting in three different stochastic wake models.

3.3.1. Uncorrelated Model

We start with an almost trivial model where the $\tilde{a}_j(t)$ are given by independent Gaussian random numbers with the mean $\tilde{\mu}_j$ and the variance $\tilde{\sigma}_j^2$. We choose $\tilde{\mu}_i = \langle a_j(t) \rangle_t = 0$. For the only free parameter $\tilde{\sigma}_j$, we choose the estimated standard deviation of the original $a_j(t)$ yielding

$$\tilde{\sigma}_j = \sqrt{\langle a_j(t)^2 \rangle_t} \, . \tag{8}$$

The wake model resulting from inserting $\tilde{a}_j$ into Equation (7) is called the *uncorrelated model* in the following. Since realisations of $\tilde{a}_j(t)$ are discontinuous time series, the *uncorrelated model* also leads to velocity fields which are discontinuous in time.

3.3.2. OU-Based Model

As a slightly more complex model, we now use an Ornstein-Uhlenbeck process (e.g., [64,65]), which is defined by

$$\dot{\tilde{a}}_j(t) = -k_j \tilde{a}_j(t) + \gamma_j \xi(t) \, , \text{ with } \langle \xi(t+\tau)\xi(t) \rangle = \delta(t-\tau) \, , \; k_j > 0 \tag{9}$$

where $\xi(t)$ is Gaussian white noise and k_j and γ_j are the parameters of the model. In this work, the integration of Equation (9) is done simply by using the analytically known two-point probability density function (pdf) (see. e.g., [65]). The correlation function of $\tilde{a}_j$ is given by:

$$c_j(\tau) := \langle \tilde{a}_j(t+\tau)\tilde{a}_j(t) \rangle_t = \frac{\gamma_j^2}{2k_j} e^{-k_j|\tau|} \tag{10}$$

with the variance $\langle \tilde{a}_j(t)^2 \rangle = \frac{\gamma_j^2}{2k_j}$ and the correlation time

$$\tau_{a_j} := \frac{2k_j}{\gamma_j^2} \int_0^\infty d\tau \, c_j(\tau) = \frac{1}{k_j} \, , \tag{11}$$

also called integral time scale. These relations can be used to estimate parameters k_j and γ_j by:

$$k_j = \frac{1}{\tau_{a_j}} \tag{12}$$

$$\gamma_j = 2\langle a_j^2(t) \rangle_t \tau_{a_j} \, , \tag{13}$$

where τ_{a_j} will be roughly estimated through $c(\tau_{a_j}) = \frac{1}{e}$.

In addition to capturing the variance of the $a_j(t)$ as in the case of the *uncorrelated model*, the Ornstein-Uhlenbeck process approximately reproduces the integral time scale of the original $a_j(t)$. However, this does not mean that the second order two-point statistics of the original $a_j(t)$ such as the auto-correlation function or the power spectral density (PSD) are also matched well, as will also be shown in Section 5.1. The stochastic wake model corresponding to the $\tilde{a}_j(t)$ described as Ornstein-Uhlenbeck processes will be referred to as the *OU-based model*. Even though time series of the Ornstein-Uhlenbeck process are continuous they are still non-differentiable due to the fast fluctuations of the white noise. The *OU-based model* therefore also yields non-differentiable velocity fields.

3.3.3. Spectral Mode

The third model we introduce is based on a parametrized PSD. The PSD of the $\tilde{a}_j$ are given by:

$$\tilde{S}^{(j)}(f) = \frac{S_0^{(j)}}{1 + \left(\frac{f}{f_{\frac{1}{2}}^{(j)}} \right)^{\alpha^{(j)}}} \tag{14}$$

with the parameters $S_0^{(j)}$ (power at zero) and $f_{\frac{1}{2}}^{(j)}$ (frequency at $\frac{S_0^{(j)}}{2}$).

For higher frequencies, $\tilde{S}^{(j)}$ behaves like a power law with an exponent given by parameter $\alpha^{(j)}$. The parameters are obtained via fitting the parametrized PSD to the estimated PSDs $S^{(j)}$ of the original $a_j(t)$. The detailed fitting procedure is described in Appendix A.1. The phases $\phi_j(f)$ of the $\tilde{a}_j$ are modelled as independent uniformly distributed random variables between 0 and 2π yielding the Fourier transform of $a_j(t)$: $\hat{\tilde{a}}_j(f) = \tilde{S}(f; S_0^{(j)}, f_{\frac{1}{2}}^{(j)}, \alpha^{(j)}) e^{i\phi(f)}$. An inverse Fourier transform yields the differentiable time series $\tilde{a}_j(t)$. The corresponding wake model, obtained from inserting the $\tilde{a}_j(t)$ into Equation (7) will be called *spectral model* in the following. Since the model is based on the PSD, it cannot only reproduce the integral time scale of the original $a_j(t)$ but also more details of the second order two-point statistics. This will be discussed further in Section 5.1.

3.3.4. Comments on More Complex Models

Our stochastic Ansatz is not principally confined to these relatively simple models for the weighting coefficients. More complex stochastic processes, as described in e.g., Friedrich et al. [66] and Kantz and Schreiber [67], could be chosen which reproduce non-linear moments of the a_j or allow for a coupling between the different weighting coefficients. However, a lot of data is needed to obtain reliable estimates of the parameters corresponding to such more complex models. Furthermore, a higher number of parameters might make it more difficult to build a practically applicable wake model.

3.4. A Spectral Surrogate in Three Dimensions

One common feature of truncated modal decompositions used in this work is that a certain fraction of turbulent kinetic energy is missing, typically on smaller scales. In order to take these small-scale dynamics into account, in Section 6 an additional turbulent field is combined with the *spectral model* introduced in the former section. The additional turbulent field is a three dimensional spectral surrogate of the original LES field confined to a central spatial region (see Section 6 for more details). Let this confined field be called $u_c(y, z, t)$. The surrogate is obtained by keeping the absolute values of the Fourier transform $|\hat{u}_c(k_y, k_z, f)|$ while substituting the phases $\phi(k_y, k_z, f)$ with uniformly distributed random numbers between 0 and 2π. An inverse Fourier transformation yields the surrogate field. This way, the PSD and all the second order correlations of the field are conserved. Spatial inhomogeneities on the other hand are lost since the spectral surrogate is a stationary and spatially homogeneous field. With this surrogate field we investigate the general possibility of using a homogeneous turbulent field.

3.5. Aeroelastic Simulations and Model Verification

Our main motivation for modelling wakes is to draw conclusions on the impact on other wind turbines. Therefore, we use aeroelastic simulations to model a wind turbine in the wake flow. For these simulations, we use the open source software FASTv7 [68], developed by NREL, and its embedded subroutines of the aerodyn code [69], which are based on the blade element momentum (BEM) theory (e.g., [70]). As inflow, we use the original LES data, truncated PODs and the output of the stochastic wake models. In this article, we use three of the multiple loads calculated by FAST,

namely the generator torque T, the rotor thrust F_t and the tower base yaw moment in z-direction t_z. The v and w components (y- and z-direction) of the inflow, which we do not model here, are set to zero. For the original simulation, setting v and w to zero lead to almost no differences in the output of FAST at least for the aspects we investigated here. It is clear that there are cases where the v, w-components become important. For such aspects our modelling procedure can be extended to these components in a similar manner. To draw conclusions on the performance of the stochastic wake models, we compare their calculated loads with the loads for truncated PODs and the original LES. Due to the stochastic character of the models, these comparisons can only be made statistically. The distribution of energy over different time scales is investigated by an estimation of the PSD, which is obtained via averaging the absolute squared Fourier spectrum over 20 windows using a cosine shaped weighting function. Furthermore, the entire energy in the load signals is compared through their variances. Subsequently, we use the algorithm given by Nieslony [71] to estimate rainflow counting histograms [72]. The rainflow counting histograms will simply be called RFCs in the following. Based on the RFC calculations, damage equivalent loads (DELs) are estimated yielding the constant load amplitude necessary to cause the same cumulative damage as the investigated load time series (for a specific number of cycles N_{eq}). The damage equivalent load is given by

$$\mathrm{DEL} = \left(\frac{\sum\limits_i n_i S_i^m}{N_{eq}} \right)^{\frac{1}{m}} . \tag{15}$$

where n_i is the number of cycles with amplitude S_i and m is the so called Wöhler exponent (e.g., [70]) Here, we choose $m = 10$, which is a typical value for materials used for WEC rotors. Since we compare the DELs resulting from reduced wake descriptions to the DEL resulting from the original LES (DEL_0), we only consider normalised DELs given by

$$\frac{\mathrm{DEL}}{\mathrm{DEL}_0} = \left(\frac{\sum\limits_i n_i S_i^m}{\sum\limits_i n_{0,i} S_{0,i}^m} \right)^{\frac{1}{m}} . \tag{16}$$

Additionally, we analyse the variance $\langle u'(y,z)^2 \rangle_t$ of the different wake descriptions since it is one of the most significant features of a turbulent wake flow. For the original LES, it has already been shown in Figure 1a. $\langle u'(y,z)^2 \rangle_t$ is also the first diagonal entry of the Reynolds stress tensor and a measure for the local average turbulent kinetic energy in the stream-wise component. In the rest of this work, it will thus be referred to as the local stream-wise kinetic energy abbreviated by SKE. In contrast to the characteristics of loads on turbines in the wake flow, $\langle u'(y,z)^2 \rangle_t$ is a property of the flow itself.

In summary, we will compare in this work different wake descriptions with the original LES based on the measures introduced above. As a direct property of the flow, the local SKE of the different descriptions is considered. The impact on a turbine in the wake is investigated based on three different loads: the generator torque, the rotor thrust and the tower base yaw moment. These loads are compared for the different wake descriptions by analysing: PSDs, RFCs, variances DELs. Truncated PODs are analysed in Section 4.2, the three different stochastic wake models in Section 5.2 and an extended stochastic wake model with added turbulence in Section 6.2.

4. Truncated PODs

In this section, we apply the POD, introduced in Section 3.2, to the LES data described in Section 2. The obtained POD modes and corresponding eigenvalues are briefly described in Section 4.1. In Section 4.2, we investigate how many POD modes are necessary to reproduce important aspects of the wake flow. For this purpose, truncated PODs (Equation (4)) including different numbers of modes are analysed via the different aspects introduced in Section 3.5.

4.1. POD Modes and Eigenvalues

We solve the eigenvalue problem in Equation (2) for the preprocessed velocity field, described in Section 3.1. This yields the eigenvalues shown in Figure 6a and the POD modes shown in Figure 7. While 10 modes capture approx. 50% of the turbulent kinetic energy of the preprocessed field, almost 100 modes are needed to capture 90% (Figure 6b). This reflects that the energy of the flow is distributed over a wide range of scales, which is a typical property of turbulent flows. The size of the structures found in the modes mostly decreases with increasing mode number, which is even more pronounced when mode numbers $j > 10$ are investigated. The modes seem more complex than those obtained in Bastine et al. [38]. This is likely to be caused by a stronger interaction with the ground since the hub height in Bastine et al. [38] was 160 m, in contrast to 90 m in the simulation here. This interaction also breaks the rotational symmetry of the wake deficit yielding statistics which are not invariant under rotations, as already visible in the variance of the field in Figure 1c. The POD modes also reveal this non-symmetric behaviour of the wake. Statistically axisymmetric fields lead to modes which are axisymmetric themselves or form statistically axisymmetric subspaces combined with other modes which have the same eigenvalue [48]. As discussed in Bastine et al. [38], mode 1 is related to the horizontal large-scale motion of the wake. The fact that we do not find a similar mode representing the motion in another direction indicates a broken axial symmetry.

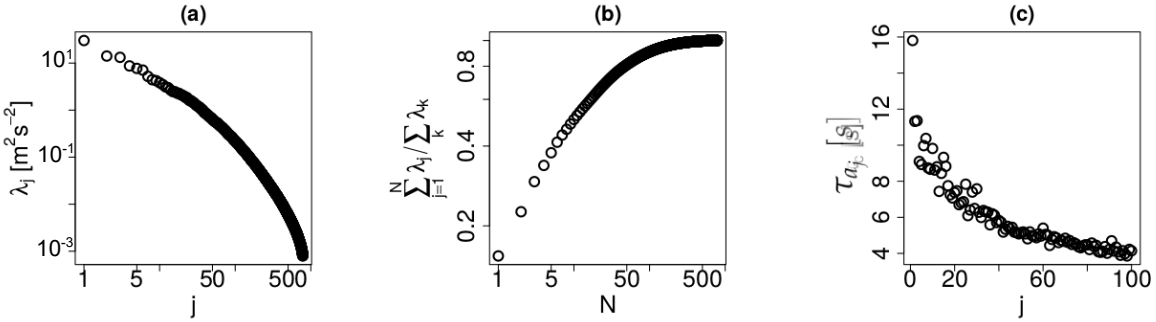

Figure 6. (**a**) POD eigenvalues; (**b**) Normalised cumulative spectrum of the POD representing the percentage of captured turbulent kinetic energy; (**c**) Integral time scale of the weighting coefficients versus mode number.

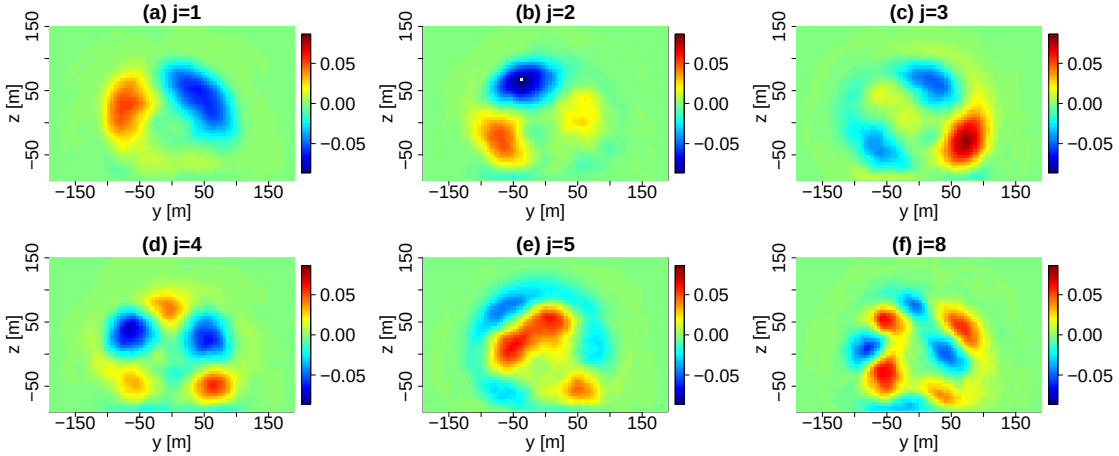

Figure 7. POD modes $\phi_j(y, z)$.

The eigenvalues presented in Figure 6a equal the variance of the weighting coefficients due to Equation (6). Thus, the energy in the fluctuations of the $a_j(t)$ also decreases with mode number. A simple quantity characterising the dynamical behaviour of the $a_j(t)$ is the integral time scale τ_{a_j} (Equation (11)) shown in Figure 6c. The integral time scale also decreases with mode number

corresponding to faster fluctuations with increasing j. Under the assumption of frozen turbulence this could also be understood as a corresponding decrease of the length scales in x-direction.

Obviously, all presented POD modes and eigenvalues are estimates since a finite number of snapshots is analysed. Most of the POD modes and eigenvalues have converged relatively well when averaging over $T > 2000$ s. However, the convergence of the modes is less good for mode numbers $j > 15$. Furthermore, using more snapshots leads to a more reliable validation, for example due to a more accurate estimation of the power spectral densities. Thus, in the rest of this work all temporal averaging $\langle \ldots \rangle_t$ is done over the complete time domain of $T = 7050$ s.

4.2. Performance of the Truncated PODs

We now use only a finite number N of the obtained POD modes (Equation (4)) as an approximate description of the original wake flow. The corresponding weighting coefficients are given by Equation (3), i.e., their temporal evolution is directly calculated from the LES data. Thus, no temporal modelling takes place. Including different numbers of modes N, the truncated PODs are now compared to the original LES based on the different aspects introduced in Section 3.5. A brief presentation of the results is followed by a more detailed discussion.

4.2.1. Results

As Hamilton et al. [39,47], we find that the spatial dependence of the local SKE $\langle u'(y,z)^2 \rangle_t$ of the wake flow can already be captured by a few modes (Figure 8), in our case approx. four modes. It can also be seen that many more modes are necessary for capturing the magnitude of $\langle u'(y,z)^2 \rangle_t$.

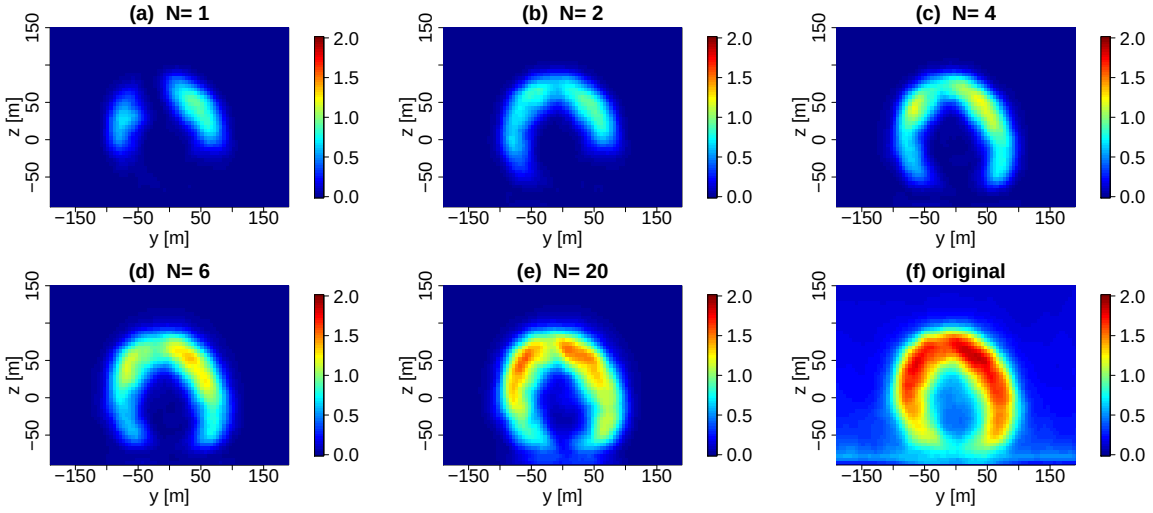

Figure 8. Local SKE $\langle u'(y,z)^2 \rangle_t$ ($m^2 s^{-2}$) for original LES and truncated PODs including different numbers of modes N.

As described in Section 3.5, the truncated PODs are also used as inflows for aeroelastic simulations. The simulated load time series of torque T, thrust F_t and tower base yaw moment t_z are shown in Figure 9. For a truncated POD with 6 modes, they roughly follow the corresponding signals of the original LES. More precisely, less than 10 modes are necessary to capture the load dynamics on large temporal scales, as illustrated through the PSDs of the loads shown in Figure 10. All PSDs show a similar behaviour with a flat region for low frequencies followed by a decay and peaks which are approximate multiples of the average rotational frequency $\langle f_{\mathrm{rot}} \rangle_t \approx 0.12$ Hz, which has been obtained from the aeroelastic simulations. The low frequency region is relatively well matched for all loads, with the weakest performance for the tower base yaw moment t_z. The small temporal scales, however, cannot be captured and thus the truncated POD misses a large part of the energy in the load signals, which can also be seen by looking at the variances in Figure 11a. For 10 modes, we get less than 60% of

the variances of F_t and t_z. Less than 90% are captured for 40 modes. For the torque T, already 20 modes will give approx. 100%.

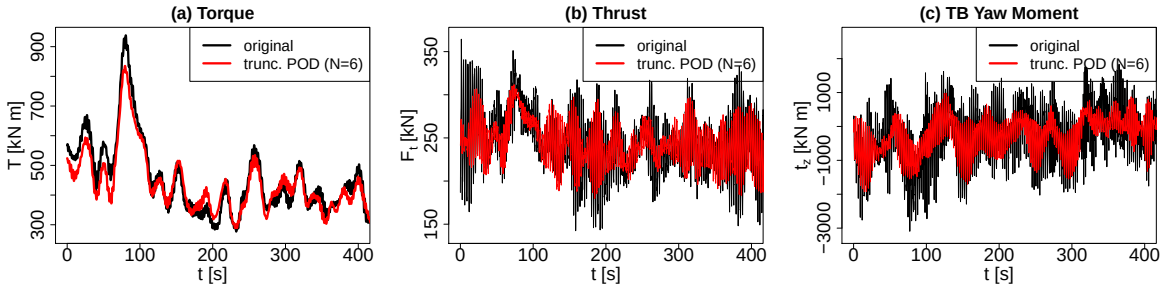

Figure 9. Time series of the different loads for original LES and a truncated POD including $N = 6$ modes. Here and in the following figures TB yaw moment is used as an abbreviation for tower base yaw moment.

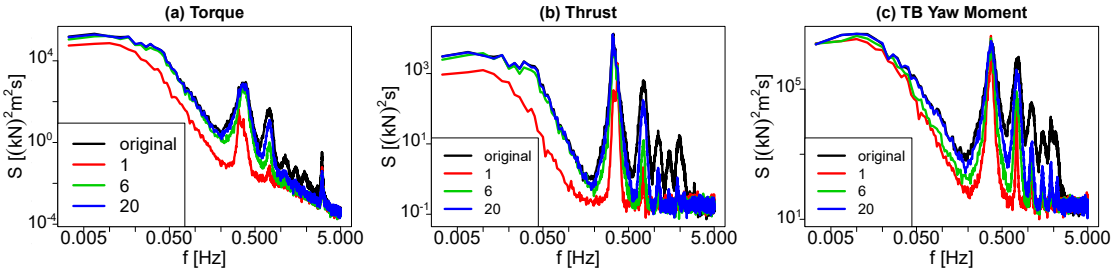

Figure 10. PSDs of the different loads for original LES and truncated PODs including different numbers of modes N.

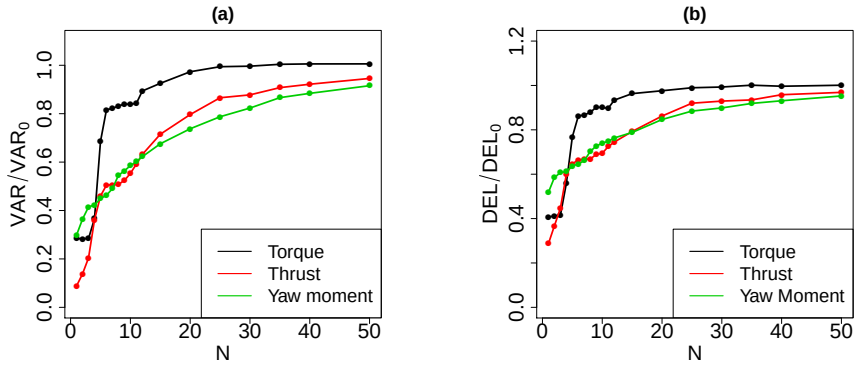

Figure 11. (**a**) Variance and (**b**) damage equivalent loads (DELs) versus the number of modes included in the truncated POD. Both are normalised by the values of the original LES.

The RFCs of the different loads are shown in Figure 12. While for T the RFCs approximately match the original loads when including 6 modes or more, strong deviations can be seen for the thrust F_t and the tower base yaw moment t_z. Particularly, the occurrence of large amplitudes cannot be captured even when including 20 modes. Consequently, a lot of modes are also needed to capture the DELs for F_t and t_z (Figure 11b). 40 modes for example yield 90% of the DEL for the original LES. As for the variance, less modes are needed for the torque T reaching more than 85% with 6 modes.

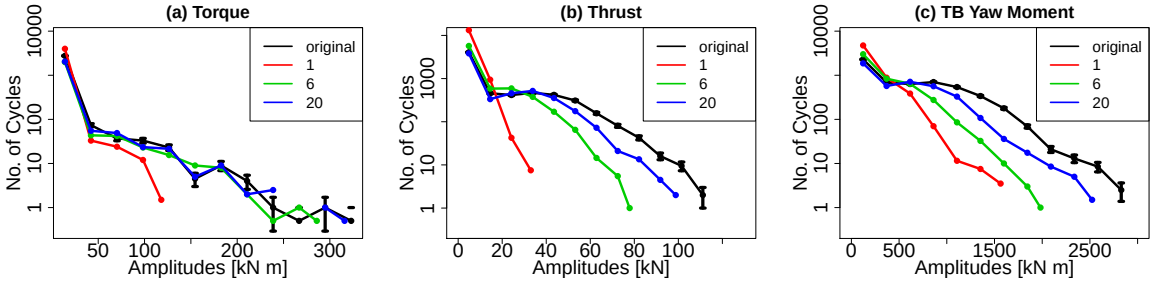

Figure 12. Rainflow counting histograms (RFCs) of different load time series for original LES and truncated PODs including different numbers of modes. To get an impression of the estimation error, the standard error shown for the original LES is estimated by $\frac{\sqrt{n_i}}{2}$ where n_i is the number of half-cycles in bin i.

4.2.2. Discussion

The interpretation of the results above is started by giving a possible explanation for capturing the spatial structure of the local SKE with only a few modes. With a few lower order modes the large scales of the wake are captured and thus the position and coarse shape of the wake can be described relatively well (see also [38]). Consequently, also the spatial dependence of the SKE is recovered. However, we cannot capture the amplitude of the SKE since the turbulent kinetic energy of the smaller scales is missing.

The dynamics of the loads is strongly influenced by the movement of the blades through the wake structures and by the temporal evolution of the wake. Thus, reproducing the large-scale structures of the wake also leads to the reproduction of the large-scale dynamics of the load time series. The discarded higher-order POD modes in a truncated POD contain only smaller structures and correspond to weighting coefficients with relatively fast dynamics. Consequently, load dynamics on large-temporal scales can be captured well in contrast to the small-scale dynamics.

The missing small-scale fluctuations in the load signals are directly related to the weak performance of the truncated PODs to reproduce variance, RFCs and DELs. Hence for the RFCs, our results also indicate that large rainflow amplitudes do not correspond to the dynamics on a specific frequency region but to the dynamics on various time scales.

The generally simpler performance for the torque might be related to the large moment of inertia of the rotor causing the higher frequencies and the occurring spectral peaks, which are poorly captured, to play a less important role. This can be seen by the relatively low frequency peaks in Figure 10a and the relatively smooth time series in Figure 9a. The more relevant low-frequency dynamics can be captured by low order POD modes corresponding to relatively large coherent structures. Hence, the time scales relevant to a specific load strongly influence the number of modes necessary for a satisfying description of this load.

The higher number of modes needed for a good large-scale description of t_z might be caused by the importance of the wake position for this load. This has been discussed in Bastine et al. [38] for a simplified measure related to t_z. It has been shown that the horizontal motion can be described qualitatively with only one specific mode but that many modes are needed to capture the amplitude of the motion.

Particularly for the generator torque, the variance and damage equivalent loads also reveal that the inclusion of some modes lead to a strong improvement while others yield almost no effect. Therefore, a further dimensional reduction might be possible by only selecting modes relevant to the specific load of interest. This has also been discussed in Bastine et al. [38], Saranyasoontorn [73,74].

In summary, we showed that relevant aspects of the wake flow could be well described by only a few modes. Particularly, the spatial dependence of the local SKE and the large temporal scales of the different load dynamics could be well captured. This is an important first step for a wake description of

reduced order and we try to reproduce these results in Section 5 using the stochastic wake models from Section 3.3. RFCs, variances and DELs of the loads are not well described with only a few modes due to the missing energy in the small scales of the wake. This aspect is further investigated in Section 6.

5. Stochastic Wake Models

In this section, three different stochastic wake models , as introduced in Section 3.3, are deduced from the LES data and their performance is investigated. In Section 5.1, the weighting coefficients $a_j(t)$ which were used in the truncated POD are analysed further to obtain the model parameters for the corresponding stochastic descriptions $\tilde{a}_j(t)$. Using the estimated parameters and resulting time series $\tilde{a}_j(t)$ in the decompositions leads to the three stochastic wake models, which are compared with the truncated POD and the original LES in Section 5.2. This comparison is done on the basis of the local SKE and the aeroelastic quantities introduced in Section 3.5.

5.1. Modeling the Weighting Coefficients $a_j(t)$

We now deduce the model parameters for the *uncorrelated model*, the *OU-based* model and the *spectral model*. Subsequently, we shortly investigate the ability of these models to capture statistical properties of the original weighting coefficients.

For the *uncorrelated model*, the $\tilde{a}_j$ are completely determined by the variance $\langle a_j(t)^2 \rangle_t$ (Figure 6a) due to Equation (8). The parameters k_j and γ_j for the *OU-based model* can be deduced from variance (Figure 6a) and integral time scales (Figure 6c) using Equation (13). For the *spectral model*, the parameters S_0, α and $f_{\frac{1}{2}}$ are obtained via fitting the parametrized Equation (14) to the estimated PSDs of the $a_j(t)$, as explained in more detail in Appendix A.1. The estimated PSDs show a qualitatively similar behaviour for all j starting with a flat region for low frequencies followed by an approximate power law behaviour (Figure 13a). This form obviously motivates the chosen parametrisation of the PSDs. given by Equation (14). An example fit is shown in Figure 13b. The estimated parameters for $j = 1, \ldots, 50$ are described in Appendix A.2.

Next, we investigate the ability of the three different models to reproduce properties of the original $a_j(t)$. Realisations of the different $\tilde{a}_j(t)$ for $j = 2$ are shown in Figure 14. The time series for the *spectral model* shows a qualitatively similar behaviour as the a_2 obtained from the LES. For the Ornstein-Uhlenbeck process a similar integral time scale can be seen but faster fluctuations play an important role yielding a non-differentiable time series. The *uncorrelated model* simply yields random numbers with the correct variance. A similar behaviour can be found for other values of j, which is chosen as an arbitrary example. In the following, variance, integral time scales and PSDs of these time series are compared.

The estimated variance $\langle a_j(t)^2 \rangle_t$ is approximately matched by all three models (Figure 15a) since all three models fulfil $\mathrm{VAR}[\tilde{a}_j] = \langle \tilde{a}_j(t)^2 \rangle_t$ by definition. The integral time scale can be approximately captured by the *OU-based* and the *spectral model*, as shown in Figures 14 and 15b. For the *uncorrelated model*, the integral time scales are exactly zero by definition.

The fitting procedure for the *spectral model* yields a good description of the PSDs up to 0.2 Hz. For $j = 2$ estimated PSDs and the analytically calculated PSDs corresponding to the estimated parameters are shown in Figures 13b and 15c, respectively. These figures show that the PSD for the *OU-based model* strongly differs from the original PSD. Thus, even though the integral time scale and variance are well matched by the *OU-based model*, the distribution of energy over the different scales is different. The uncorrelated model yields a trivial PSD also failing to reproduce the PSD of a_2. Similar results as for $j = 2$ are found for other mode numbers.

Overall, the *spectral model* leads to the best statistical reproduction of the original a_j yielding smooth differentiable time series with similar second order two-point statistics. This is expected since it is the most complex model using three parameters to fit the original data.

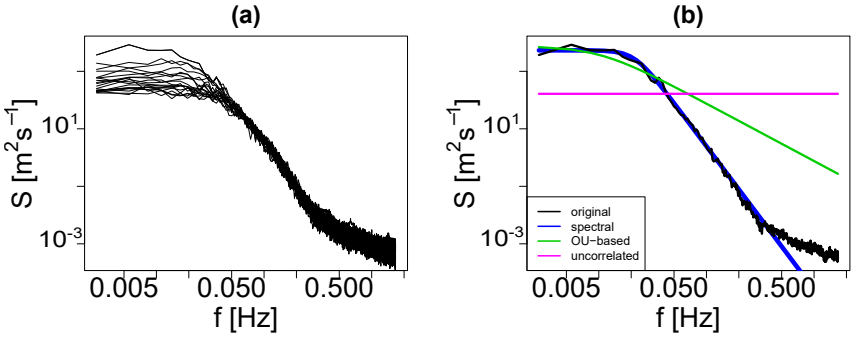

Figure 13. (**a**) PSDs of the weighting coefficients $a_j(t)$ for $j = 1, 2, \ldots, 50$; (**b**) PSD for $a_2(t)$ and the corresponding fit for the *spectral model*. Additionally, analytical PSDs for *uncorrelated* and *OU-based model* are shown corresponding to the estimated model parameters of these models.

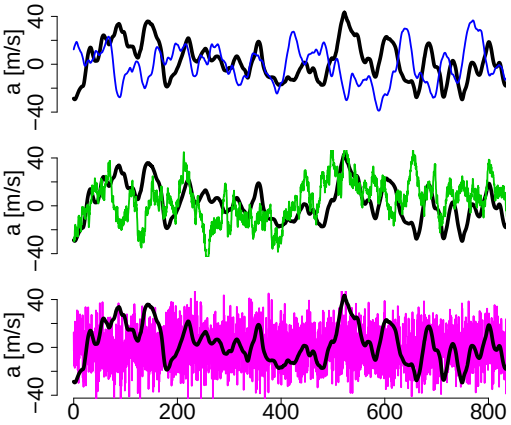

Figure 14. Time series of $a_2(t)$ (black) and the different stochastic models $\tilde{a}_2(t)$. From top to bottom: *spectral model* (blue), *OU-based model* (green) and *uncorrelated* model (magenta).

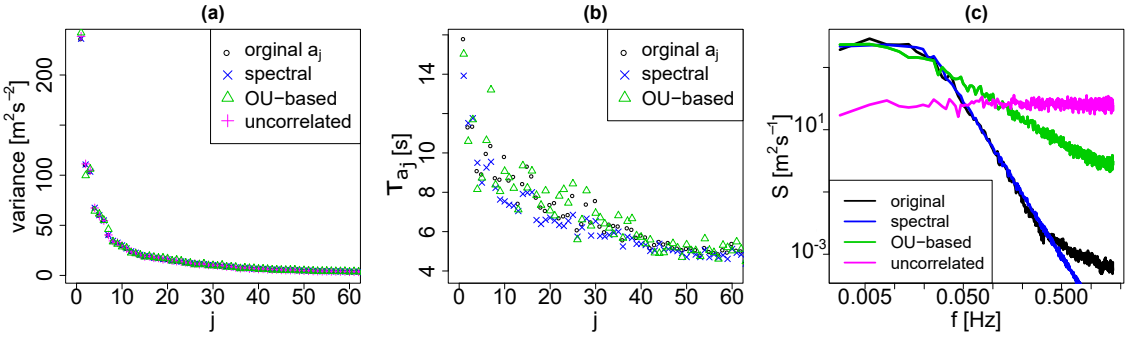

Figure 15. Properties of the weighting coefficients $a_j(t)$ and the stochastic models $\tilde{a}_j(t)$: (**a**) Variance versus mode number j; (**b**) Integral time scales versus mode number. The results for the *uncorrelated model* are not shown since the integral time scale is zero for all j; (**c**) Estimated PSDs of $a_2(t)$ and realisations of the different stochastic models $\tilde{a}_2(t)$.

5.2. Performance of the Stochastic Wake Models

Based on the model parameters estimated above, we can now generate random time series $\tilde{a}_j(t)$ and insert them into Equation (7) yielding realisations of the corresponding stochastic wake models, introduced in Section 3.3. In this section, we investigate the performance of these models with respect to the aspects specified in Section 3.5. A brief presentation of the results is followed by a more detailed discussion.

5.2.1. Results

The $\tilde{a}_j(t)$, used for the stochastic wake models, aim for capturing statistical properties of the $a_j(t)$ used in the truncated POD. Therefore, a stochastic wake model $\tilde{u}^{(N)}$ including N modes performs well if it yields similar results as the corresponding truncated POD $u^{(N)}$. Hence, we compare the outcome for the truncated POD and the different stochastic wake models for a fixed number N. The results of the original LES are included to indicate the performance of the truncated POD.

Since we cannot illustrate all choices of N separately, we choose a fixed value of $N = 6$ as an example. This choice is motivated by the fact that for the truncated POD six modes already show some promising results, as discussed in Section 4.2. Similar results, however, have been found for all $N < 15$. Later in this section, the performance of the *spectral model* will also be investigated for varying N.

The local SKE $\langle \tilde{u}'(y,z)^2 \rangle_t$ looks very similar for the truncated POD and all three stochastic wake models (Figure 16) showing only minor quantitative differences, which could be caused by statistical fluctuations.

The PSDs of the time series, shown in Figure 17, reveal different behaviour for the different models. While the *spectral model* coincides with the truncated POD, the *OU-based model* shows significant differences. Particularly, it has a smaller slope around 0.1 Hz and underestimates the energy in the low frequency regime. On the other hand, the width and height of the peak at $3 \cdot \langle f_{\mathrm{rot}} \rangle_t$ are relatively well matched. As expected, the *uncorrelated model* fails almost completely to reconstruct the PSD. Sections of the corresponding load time series can be found in Figure A2 in the Appendix B.

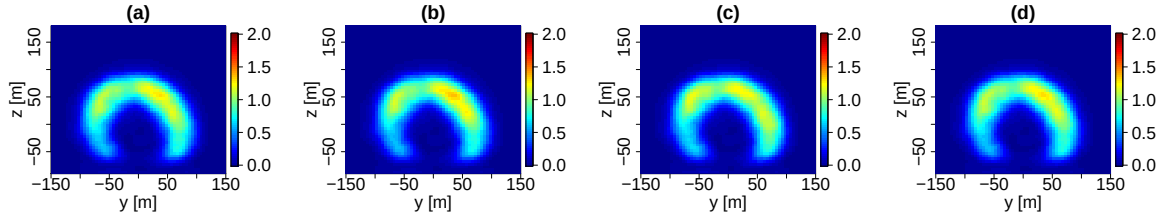

Figure 16. Local SKE $\langle u'(y,z)^2 \rangle_t$ ($\mathrm{m^2 s^{-2}}$) using $N = 6$ POD modesfor truncated POD and the different stochastic wake models: (**a**) truncated POD; (**b**) *spectral model*; (**c**) *OU-based model*; (**d**) *uncorrelated model*.

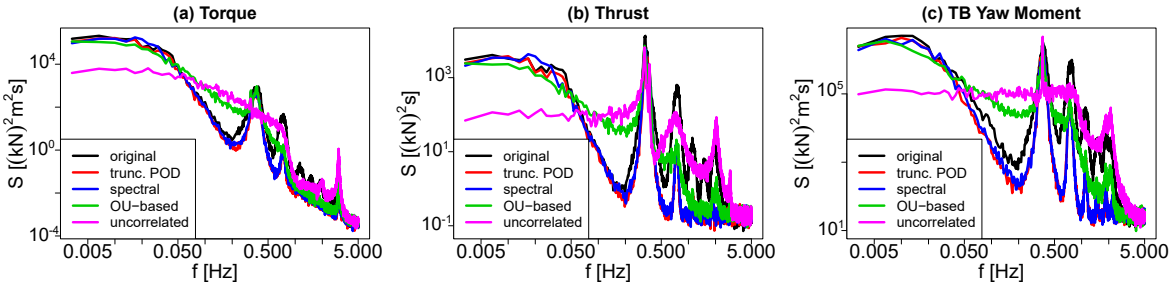

Figure 17. PSDs of the different loads for original LES and the different wake descriptions using $N = 6$ POD modes. Note that we aim to capture the behaviour of truncated PODs here, as pointed out in the beginning of this section.

Examining the RFCs in Figure 18, the *uncorrelated model* also shows a strongly different behaviour than the truncated POD. The RFCs for *spectral* and *OU-based model* approximately coincide with the RFC of the truncated POD. Differences for the *OU-based model* can only be suspected and do not seem to be significant.

For the *spectral model*, we also investigate the behaviour for different numbers of included modes with respect to the variance and DELs, as shown in Figure 19. For less than ten modes, truncated POD and stochastic model show similar results. For higher mode numbers, variance and DELs of the rotor

torque T appear to be underestimated by the model while a slight overestimation is present for the thrust F_t. However, also larger estimation errors are present for higher mode numbers. The errors shown are estimated as the standard deviation for an ensemble of 10 realisations of the *spectral model*, calculated for $N = 1, 4, 5, 6, 10, 30$. It should be noted that the statistical estimates for the truncated PODs also have errors. Due to the highly turbulent nature of the flow, every LES simulation would lead to slightly different values. However, these errors are much more difficult to estimate. Running an ensemble of LES, for example, is computationally too expensive and other statistical methods lead to unreliable estimates.

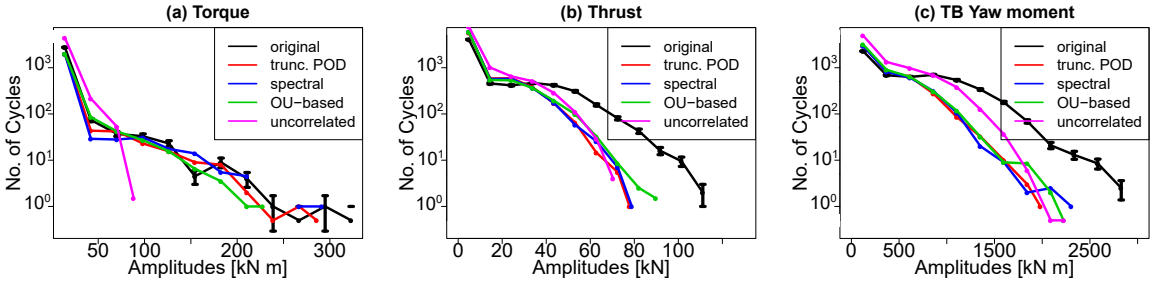

Figure 18. RFCs of the different loads for the original LES and the different wake descriptions using $N = 6$ POD modes. To get an impression of the estimation error, the standard error is shown for the original LES. It is estimated by $\frac{\sqrt{n_i}}{2}$ where n_i is the number of half-cycles in bin i. Note that we aim to capture the behaviour of truncated PODs here, as pointed out in the beginning of this section.

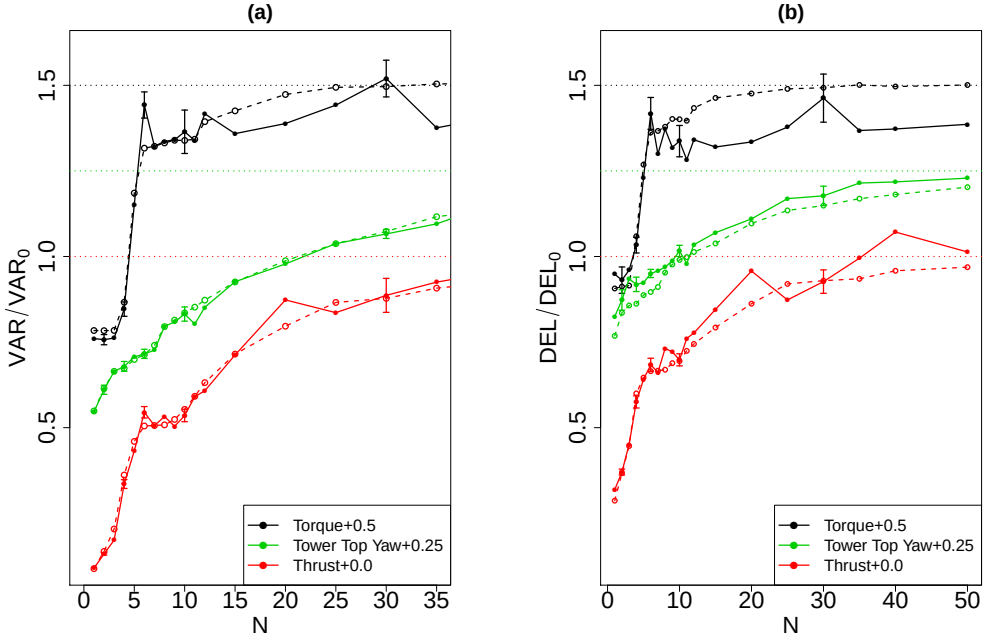

Figure 19. (**a**) Variance and (**b**) DELs for different loads versus no. of modes N included in the wake descriptions. The solid lines with filled circles represent the results for the *spectral model* while the dashed lines show the results for the truncated POD. The curves for the different loads are vertically shifted for a better visualisation, as described in the legend. The corresponding shifted values representing 1.0 are illustrated by the dotted lines. Standard errors are shown for the *spectral model* for $N = 2, 4, 6, 10, 30$. They are estimated through the standard deviation from an ensemble of 10 realisations.

5.2.2. Discussion

Our results show that modelling the weighting coefficients as independent stochastic processes can lead to similar statistical results as obtained when using the original weighting coefficients used in the truncated POD. Dependent on the quantities, a model aims to reproduce, stochastic processes of different complexity might be needed.

The local SKE is reproduced even by all three investigated processes. This result is caused by the fact that $\langle \tilde{u}'(y,z)^2 \rangle_t$ depends only on the variance of the weighting coefficients due to:

$$\begin{aligned} &\langle \tilde{u}'(y,z)^2 \rangle_t \\ &\quad = \Big\langle \sum_{i=1,j=1}^{N} \tilde{a}_i(t)\tilde{a}_j(t)\phi_i(y,z)\phi_j(y,z) \Big\rangle_t = \sum_{i=1,j=1}^{N} \langle \tilde{a}_i(t)\tilde{a}_j(t) \rangle_t \phi_i(y,z)\phi_j(y,z) \\ &\quad = \sum_{i=1,j=1}^{N} \langle \tilde{a}_i(t)^2 \rangle_t \delta_{ij} \phi_i(y,z)\phi_j(y,z) = \sum_{i=1}^{N} \langle \tilde{a}_i(t)^2 \rangle_t \phi_i(y,z)^2 \,. \end{aligned} \tag{17}$$

Since the variance of the a_j is approximately matched by the $\tilde{a}_j$ of all three stochastic wake models, the local SKE is matched as well.

In contrast to the local SKE, the spectral characteristics of the loads on a wind turbine can be captured well only by the *spectral model*, which also captures the spectral characteristics of the $(a_j(t))_{j=1}^{N}$. Hence, detailed spectral properties of the a_j play an important role in this case. This seems to be different in the frequency region around $3\langle f_{\mathrm{rot}} \rangle_t$, since the *OU-based model* also performs quite well here.In this region, the loads are dominated by the movement of the rotor blades through the flow structures and thus capturing the persistence time of these structures plays a major role. This persistence time of the different structures is closely related to the integral time scale of the weighting coefficients. Since the *OU-based model* offers a good approximation of these time scales, it shows a good performance around $3\langle f_{\mathrm{rot}} \rangle_t$.

For the RFCs, matching the variance and integral time scale of the $a_j(t)$ might also be sufficient since *spectral model* and *OU-based model* also performed relatively well. Possibly, the rotation of the blades through the wake field plays a dominant role for the appearing cycles in the time series. In other words, the spatial characteristics of the flow in the yz-plane might be more important than the temporal characteristics or the characteristics in the x-direction. This might, however, differ strongly for different loads.

The satisfying performance of the *spectral model* for $N \leq 10$, as illustrated by variance and DELs, shows that our results are not confined to the case of $N = 6$.

It is difficult to identify the reason for the possibly weaker performance for the torque when including more modes. One possible explanation might be that the parametrisation of the PSD or the fitting procedure might perform worse for higher mode numbers ($j > 15$). However, preliminary experiments with spectral surrogates of the a_j, which match the PSD exactly, indicate similar trends. Another reason could be that the assumption of independence of the a_j becomes problematic when including many modes.

It should be noted that the stochastic wake models, presented in this section, still have the same shortcomings as the truncated POD, namely the missing energy for small-scale dynamics when including only a few modes. Consequently, the fatigue of a wind turbine component will in most cases be severely underestimated if the estimation is solely based on these low order stochastic models. Thus, in the next section we investigate an approach to include small-scale structures without the inclusion of a large number of modes.

6. A Stochastic Wake Model with Added Turbulence

As discussed in the former sections, we need many modes (more than 30) to capture the load behaviour on small time scales and consequently also for the variance and DELs. Including many

modes leads to many model parameters, which makes it difficult to build simple and practically applicable models. One way of reducing the number of model parameters might be to parametrise the parameter's dependence on the mode number (e.g., Figure A1 for the *spectral model*). However, for such a simplification, the stochastic wake models might show a weaker performance when taking many modes into account, as discussed in Section 5.2. Furthermore, higher order POD modes are hard to estimate from data. In this section, we examine a different approach, describing the large-scale and small-scale dynamics of the wake separately by combining the *spectral model* including a few modes with an additional homogeneous turbulent field. Similar approaches have been used in [28–31,39]. We start by illustrating the basic idea and underlying hypothesis of our approach in Section 6.1. Subsequently, the performance of the extended *spectral model* with added turbulence is investigated via the different aspects introduced in Section 3.5.

6.1. Basic Idea

In Section 4.2, we hypothesised that a few POD modes can qualitatively capture the statistical inhomogeneities of the wake flow, as illustrated by the local SKE of truncated PODs in Figure 8. The magnitude of the enhanced turbulence in the outer region of the wake cannot be reproduced due to missing small-scale structures in the wake deficit. Thus, here we try to capture these structures by adding a homogeneous turbulent field to the *spectral model*. As the additional turbulent field we use a spectral surrogate of the flow field in the wake centre, as marked by the small black circle in Figures 1c and 3c. The surrogate field is shown in Figure 20. Such a spectral surrogate, as introduced in Section W, can be understood as a homogeneous approximation of the turbulent field in the wake centre. This way we can conveniently test if a homogeneous field is principally able to capture the missing small-scale turbulence. We only use the small central region since it is almost always covered by the deficit and thus less influenced by the ambient field. In principle, other turbulence models such as [75] could be used to model the homogeneous field but in this case, we would investigate the ability of such approaches to reproduce the turbulence in the LES simulation, which is not our goal here and beyond the scope of this work.

The extended *spectral model* is now built as follows. The wake deficit is extracted by the same procedure as used for the preprocessing of the field, which is described in Section 3.1. We add the homogeneous turbulent field inside the identified wake structure while outside the ABL flow from the LES is used, which is uninfluenced by the turbine. A snapshot of the resulting field is shown in Figure 21. It should be noted that this approach neglects the interaction of the ABL the with the wake region and thus has to be justified by its performance.

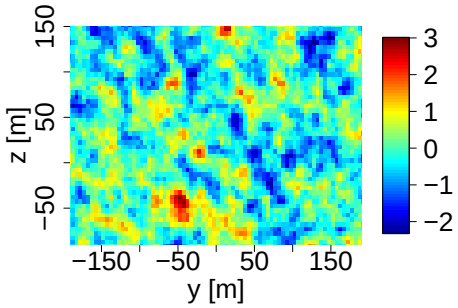

Figure 20. Homogeneous turbulent field: A spectral surrogate from the central wake region marked by the black circles in Figures 1c and 3c.

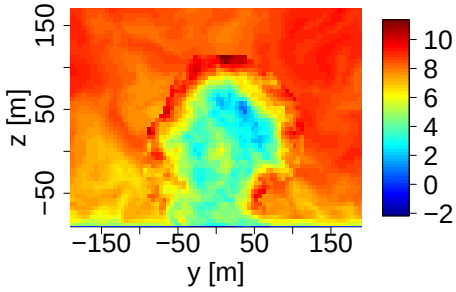

Figure 21. Snapshot of the *spectral model* with added small-scale turbulence (Figure 20) in the wake and ambient ABL turbulence outside the wake structure.

6.2. Performance

Next, we investigate the performance of the *spectral model* combined with the additional turbulent field. A brief presentation of the results is followed by a short discussion.

6.2.1. Results

The local SKE of the field for different numbers of modes is shown in Figure 22. For 6 modes, it is very similar to the original local SKE shown in Figure 1c, not only with respect to its spatial structure as for the truncated POD (Figure 8) but also with respect to its magnitude. Including much more modes leads to an overestimation of the local SKE.

Including the turbulent field leads to a good match of the PSDs for higher frequencies (Figure 23) in contrast to the results for the unextended *spectral model* (Figure 17) or the truncated POD (Figure 10). This can even be seen when using only the spectral surrogate without any additional modes. In this case however, the low frequencies cannot be matched. With 6 modes low and high frequencies seem to be matched pretty well. This is also indicated by the load time series shown in Figure A3 in the Appendix B.

Concerning the RFC analysis, no good modelling for thrust and tower base yaw moment could be obtained by our POD approach (Figures 12 and 18) up to here. After adding the turbulent field more cycles with high amplitudes are found in the RFCs, as shown in Figure 24. The model with zero modes differs strongly from the original LES for all different loads. Six modes seem to perform best for thrust while about 20 modes are favourable for the tower base yaw moment.

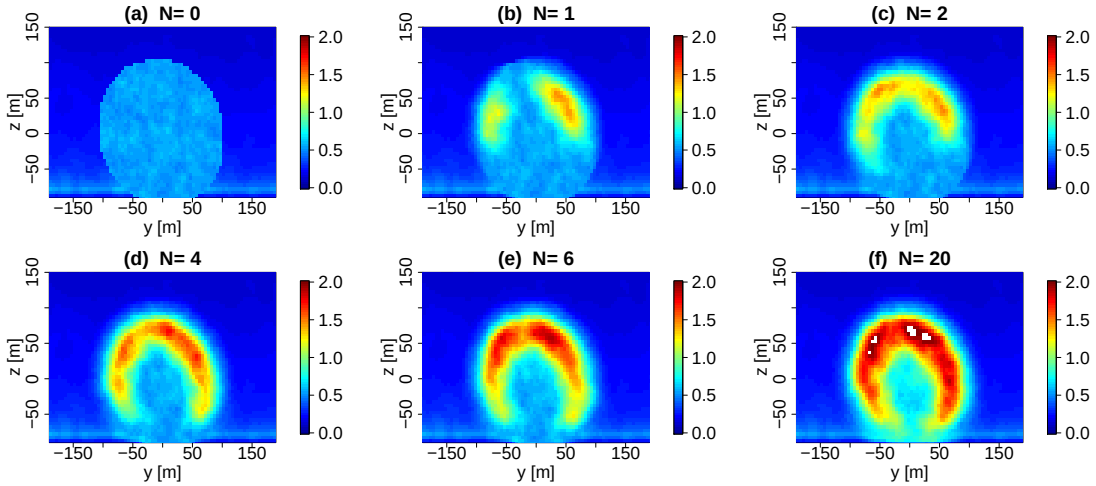

Figure 22. Local SKE $\langle u'(y,z)^2 \rangle_t$ $(\mathrm{m^2 s^{-2}})$ for original LES and the *spectral model* with added turbulence including different numbers of modes N.

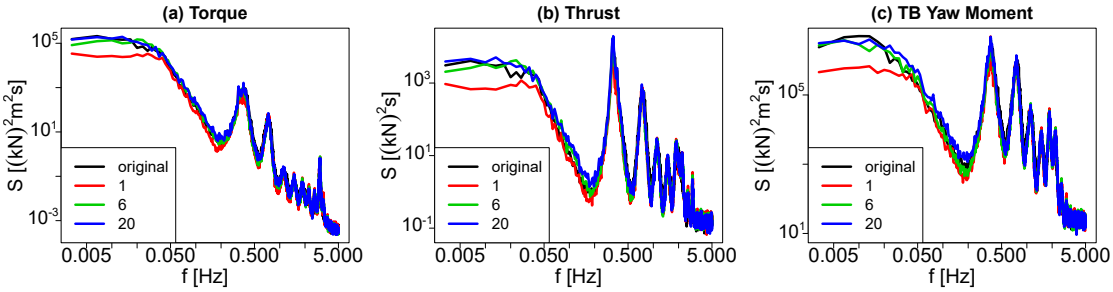

Figure 23. PSDs of the different loads for original LES and *spectral model* with added turbulence including different numbers of POD modes.

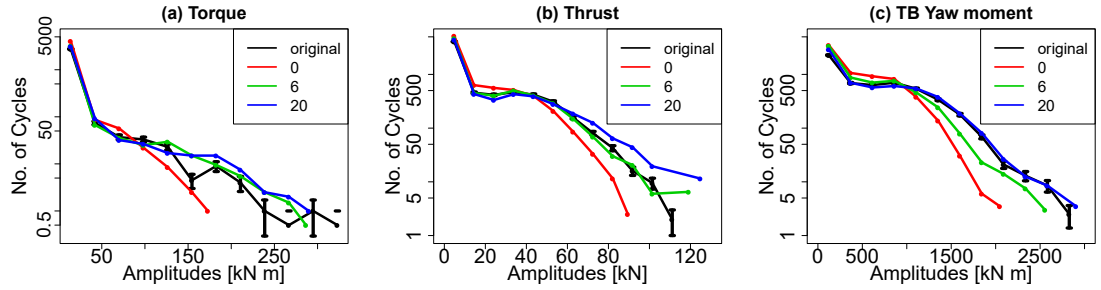

Figure 24. RFCs for different loads and different numbers of modes included in the *spectral model* with added turbulence.

For torque and thrust, variance and damage equivalent loads show relatively good agreement with the original LES when including around $6-10$ modes according to Figure 25. More modes are needed for the tower base yaw moment. Including many more modes leads to strong over-estimations for all loads, as we will discuss below.

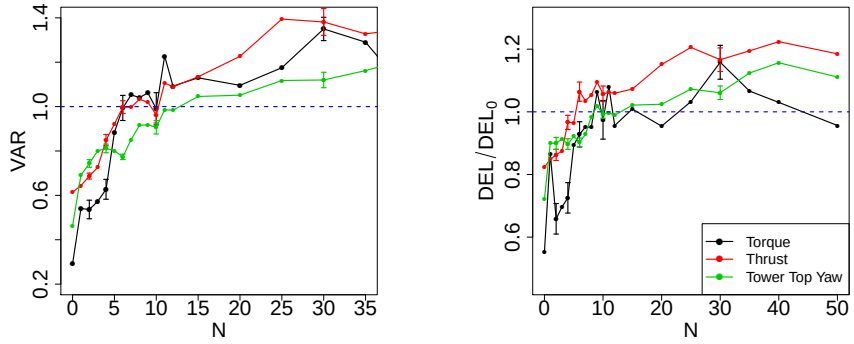

Figure 25. Variance and DELs for different loads versus no. of modes included in the *spectral model* with added turbulence. Standard errors are shown for the *spectral model* for $N = 2, 4, 6, 10, 30$. They are estimated from the standard deviations from an ensemble of 10 realisations.

6.2.2. Discussion

We start the discussion of the results above by considering the local SKEs, which indicate that the statistical inhomogeneities in the field can be reproduced nicely by 6–10 modes. Interestingly, 6–10 modes also seem to perform well or best for most of the other measures such as the PSDs, RFCs, variance, or DELs of the different loads. This indicates that most relevant large-scale effects are captured by 6 modes while the small-scale effects are captured by the homogeneous turbulent field,

which is moving with the wake structure. Similarly, Hamilton et al. [47] found that lower order POD modes are responsible for the anisotropy in the wake while the higher order modes mostly contribute to higher-order and small-scale turbulence. There is however a fundamental difference in our approach since we add the homogeneous field only to the instantaneous wake deficit and not to the ambient field. This way adding a homogeneous field still increases the overall anisotropy. This explains why a relatively small number of modes might be enough in our setting.

The over-estimations for higher numbers of included modes, observed particularly for the variances and DELs or the RFCs of the thrust, are caused by the fact that higher order modes describe small-scale structures which are also included in the added turbulent field. Thus, further adjustments of the turbulent field and the selected modes are needed. The weaker performance for the tower base yaw moment, when using 6 POD modes, appears to be caused by the fact that the truncated decompositions struggle to capture wake structures which have moved far away from the mean position of the wake, as also discussed in Section 4.2 and Bastine et al. [38].

Overall, we can conclude that including the missing small-scale energy through an an additional homogeneous turbulent field is a promising idea. Since not all loads are well described using 6–10 modes, for future work it could be helpful to compensate the overestimation of the load variability when including more modes than 6–10. Simply adapting the level of turbulence through a scalar is probably not sufficient. The included modes add energy in a bounded frequency range while the scalar leads to a broad addition or reduction of energy.

As mentioned before, other more sophisticated homogeneous fields could be used instead of the surrogate field such as found in Mann [75] and Kleinhans [76]. However, as also indicated by [34], it might be possible that wake turbulence might be modelled similar to ideal homogeneous isotropic turbulence quite independently from the ambient flow.

7. Conclusions

In this work we presented a conceptional approach to derive stochastic reduced order wake models from costly CFD calculations such as LES simulations. Such expensive computations can be done on big computer clusters in reasonable times only for several hours of operation of a turbine. We show that a strong reduction of complexity is possible and important aspects of the wake flow and its impact on a wind turbine can principally be reproduced by relatively simple models. The corresponding wake flows can be generated in a very fast stochastic manner enabling, for example, long-term studies of e.g., load assessments. In contrast to a general model reduction of a wake flow, we show that the necessary complexity of the wake models strongly depends on the quantities the models should be able to reproduce. This is not only true for the necessary number of modes, as also discussed in Bastine et al. [34] and in Saranyaoontorn [73,74], but also for the complexity of the stochastic models describing the temporal dynamics through the weighting coefficients $a_j(t)$. Hence, our approach allows to build models which are as complex as necessary but as simple as possible with respect to a specific application, i.e., the loads or other quantities the models should be able to reproduce. For example, in order to reproduce the DEL of the original LES for the rotor thrust within a few percent, approximately 6–10 POD modes plus a homogeneous turbulent field were necessary. Obviously, our ideas have to be tested and extended for different atmospheric situations, different wind turbines or distances from the turbine. Deducing simplified models in this huge corresponding parameter space is a very challenging task. However, in the design process of wind turbines for example, efficient stochastic models corresponding to important cases of wake flows can be very useful.

As this work is mainly a proof of concept, our analysis is confined to a two-dimensional cross section. Since a wind turbine operates in such a plane this might lead to the simplest model possible. An extension to a three-dimensional domain, however, is straightforward and might lead to more general wake descriptions. It should therefore be investigated in further research.

The described procedure to obtain reduced order models is not principally confined to data from computational simulations. Further investigations using for example high-speed PIV measurements in

laboratory wake flows would be very interesting. Due to their growing potential also lidar scanners could offer complementing measurements in the near future, e.g., following ideas presented by Beck et al. [77] and Barthelmie et al. [78].

As discussed, for example, in Section 4.2, the POD-based approach has difficulties to capture large amplitudes of the meandering motion. Thus, another possible improvement of our model could be the inclusion of the meandering motion through an additional model, such as the DWM [28–31]. In the DWM, the meandering caused by large atmospheric structures is the only large-scale effect which is modeled explicitly and thus a POD-based approach is a promising extension. In this case, the POD-based approach would have to be performed in the meandering frame of reference. Furthermore, our model should be compared to very recent approaches by Doubrawa et al. (2016), which stochastically model the wake structure based on spectral descriptions of its edges.

The results of our work also confirm that not only the large scales of the wake are relevant but that also the small-scale structures play a very important role, e.g., for capturing the RFCs of a load time series. We demonstrate that the small scales can be captured by adding a homogeneous turbulent field to our model while the large scales are captured by a few POD modes. Our approach, as well as others such as the DWM [28–30], can therefore strongly benefit from a good description of small-scale wake turbulence. Hence, its detailed investigation, as for example found in [33,34,55,79–81], is a very essential area of research for the improvement of future dynamic wake models.

In the end, we would like to stress that the idea of combining modal decompositions, such as the POD, with stochastic models is not only applicable to wind turbine wakes. In principle it might be of use for the description of any complex dynamical system, as for example given by fluid flows.

Acknowledgments: We would like to acknowledge fruitful discussions with Philip Rinn, Björn Witha, Pedro Lind, Hauke Beck, Christian Behnken, Davide Trabucchi and Juan Jose Trujillo from ForWind Oldenburg). This work has been funded by the Bundesministerium für Wirtschaft und Energie (BMWi) due to a decision of the German Bundestag (FKZ0325397A) and by the Lower Saxony Ministry of Science and Culture within the project "ventus efficiens".

Author Contributions: David Bastine performed the analysis and wrote the major part of this article. Joachim Peinke and Matthias Wächter are supervisor and co-supervisor of David Bastine and his Ph.D. work. Therefore, they helped with the ideas and discussions and proofread the manuscript. Lukas Vollmer performed the LES simulations and mainly wrote the part describing the LES data.

Conflicts of Interest: The authors declare no conflict of interest.

Appendix A. Details of the Spectral Model

Appendix A.1. Fitting Procedure

As shown in Figure 13a the PSDs $S^{(j)}$ of the original $a_j(t)$ show a qualitatively similar behavior for all j and can be described well by the parametrized PSD $\tilde{S}^{(j)}(f_i^{(j)}; S_0^{(j)}, \alpha^{(j)}, f_{\frac{1}{2}}^{(j)})$ given by Equation (14).

The parameters $S_0^{(j)}$, $\alpha^{(j)}$ and $f_{\frac{1}{2}}^{(j)}$ are estimated using least squares in a logarithmic framework. This means they are obtained by minimizing $\sum_{i=1}^{N} (\log(S_i) - \log(\tilde{S}_j(f_i; S_0^{(j)}, \alpha^{(j)}, f_{\frac{1}{2}}^{(j)})))^2$ with respect to $S_0^{(j)}, f_{\frac{1}{2}}^{(j)}, \alpha^{(j)}$, where $S_i^{(j)}$ and $f_i^{(j)}$ are the PSD and frequency values obtained through the statistical estimation from the LES data. While this procedure yields satisfying estimates of $\alpha^{(j)}$ and $f_{\frac{1}{2}}^{(j)}$, $S_0^{(j)}$ is systematically underestimated due to the nonlinear weighting by the logarithmic function. We circumvent this problem by choosing $S_0^{(j)}$ to be the value which yields the estimated variance of the $a_j(t)$: $\mathrm{VAR}[\tilde{a}_j(t; S_0, \alpha, f_{\frac{1}{2}})] = \langle a_j(t)^2 \rangle_t$, where $\alpha, f_{\frac{1}{2}}$ are taken from the logarithmic fit. An example fit is shown in Figure 13b. It should be noted that alternative fitting procedures are also possible and lead to similar results as long as the PSD is matched well in all the frequency ranges and not only for low or high frequencies.

Fitting in a logarithmic framework is a very common procedure to find power law exponents or damping coefficients in exponential functions. However, the logarithmic function introduces a nonlinear weighting to the least squares fit. Therefore, large values of the S_i have less influence than for a fit without log. One resulting problem is for example that when fitting to a constant function or constant region of a function, the fit will lead to an underestimation in this region, since positive deviations are weighted weaker than negative ones. That is why we estimated S_0 separately.

Appendix A.2. Estimated Parameters

The estimated parameters for varying j are shown in Figure A1. S_0 shows a fast decrease with mode number. Therefore, the decrease of the variance of the a_j with j is mainly related to a decrease of fluctuations on large temporal scales. The power law exponent α shows a negative trend yielding a slight increase for the energy related to higher frequencies. The increase of $f_{\frac{1}{2}}$ is related to a decrease of the integral time scale τ_{a_j} of the a_j.

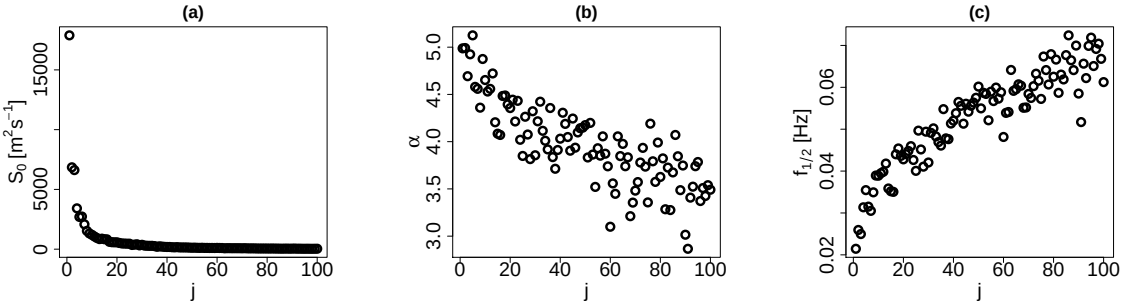

Figure A1. Estimated parameters for the *spectral model* versus the mode number j.

Appendix B. Time Series of Loads

In this appendix we present sections of the load time series used in our statistical analysis. In Figure A2 the load time series resulting from the truncated POD are compared with the results from the different stochastic models. Six POD modes have been used ($N = 6$). Only a first visual impression can be given by such pictures showing only one short section of the series. Thus, a quantitative comparison using different statistical measures has been done in Section 5.2.

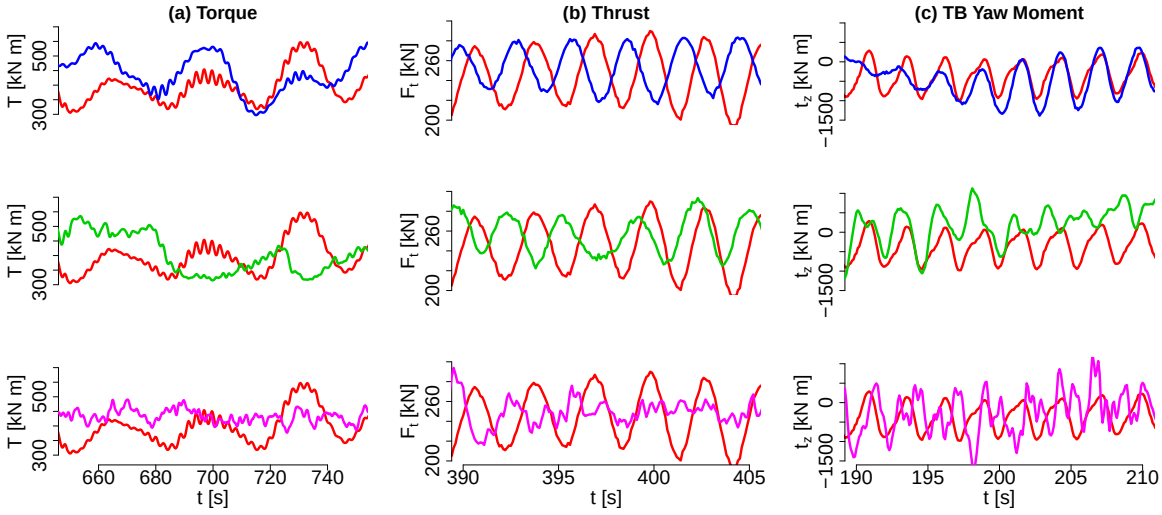

Figure A2. Sections of the time series of the different loads for the truncated POD (red) with $N = 6$ compared to *spectral model* (blue), *OU-based model* (blue), *uncorrelated model* (magenta).

In Figure A3 load time series resulting from the original LES are compared with the results from the extended *spectral model* ($N = 6$) with added turbulence. The time series indicate very similar statistical behavior, which could be confirmed by quantitative measures in Section 6.2.

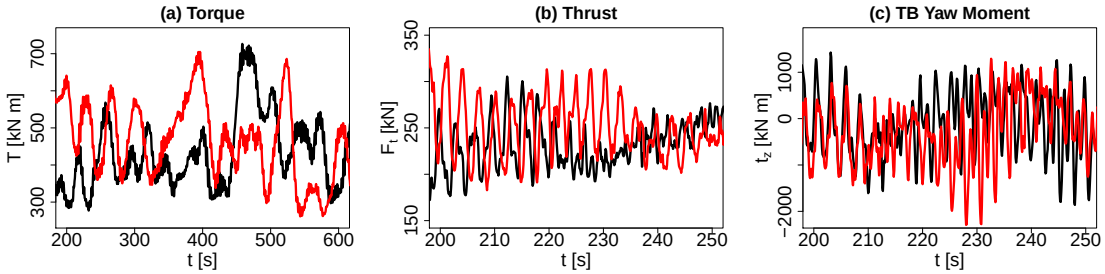

Figure A3. Sections of the time series of the different loads for original LES and for the *spectral model* with added turbulence including $N = 6$ modes.

References

1. Barthelmie, R.J.; Frandsen, S.T.; Nielsen, M.; Pryor, S.; Rethore, P.E.; Jørgensen, H.E. Modelling and measurements of power losses and turbulence intensity in wind turbine wakes at Middelgrunden offshore wind farm. *Wind Energy* **2007**, *10*, 517–528.
2. Barthelmie, R.J.; Pryor, S.C.; Frandsen, S.T.; Hansen, K.S.; Schepers, J.G.; Rados, K.; Schlez, W.; Neubert, A.; Jensen, L.E.; Neckelmann, S. Quantifying the Impact of Wind Turbine Wakes on Power Output at Offshore Wind Farms. *J. Atmos. Ocean. Technol.* **2010**, *27*, 1302–1317.
3. Frandsen, S. *Turbulence and Turbulence Generated Fatigue in Wind Turbine Clusters*; Risø-R 1188; Risø National Laboratory: Roskilde, Denmark, 2005.
4. Barthelmie, R.J.; Hansen, K.; Frandsen, S.T.; Rathmann, O.; Schepers, J.G.; Schlez, W.; Phillips, J.; Rados, K.; Zervos, A.; Politis, E.S.; et al. Modelling and Measuring Flow and Wind Turbine Wakes in Large Wind Farms Offshore. *Wind Energy* **2009**, *12*, 431–444.
5. Chowdhury, S.; Zhang, J.; Messac, A.; Castillo, L. Unrestricted wind farm layout optimization (UWFLO): Investigating key factors influencing the maximum power generation. *Renew. Energy* **2012**, *38*, 16–30.
6. Gonzalez, J.S.; Payan, M.B.; Santos, J.M.R.; Gonzalez-Longatt, F. A review and recent developments in the optimal wind-turbine micro-siting problem. *Renew. Sustain. Energy Rev.* **2014**, *30*, 133–144.
7. Schmidt, J.; Stoevesandt, B. Wind Farm Layout Optimisation Using Wakes from Computational Fluid Dynamics Simulations. In Proceedings of the EWEA Conference, Barcelona, Spain, 10–13 March 2014.
8. Corten, G.; Schaak, P. Heat and flux: increase of wind farm production by reduction of the axial induction. In Proceedings of the European Wind Energy Conference, Madrid, Spain, 16–19 June 2003.
9. Fleming, P.A.; Gebraad, P.M.O.; Lee, S.; van Wingerden, J.W.; Johnson, K.; Churchfield, M.; Michalakes, J.; Spalart, P.; Moriarty, P. Evaluating techniques for redirecting turbine wakes using SOWFA. *Renew. Energy* **2014**, *70*, 211–218.
10. Annoni, J.; Gebraad, P.M.O.; Scholbrock, A.K.; Fleming, P.A.; van Wingerden, J.W. Analysis of axial-induction-based wind plant control using an engineering and a high-order wind plant model. *Wind Energy* **2016**, *19*, 1135–1150.
11. Gebraad, P.M.O.; Teeuwisse, F.W.; van Wingerden, J.W.; Fleming, P.A.; Ruben, S.D.; Marden, J.R.; Pao, L.Y. Wind plant power optimization through yaw control using a parametric model for wake effects-a CFD simulation study. *Wind Energy* **2016**, *19*, 95–114.
12. Ferrer, E.; Browne, O.M.; Valero, E. Sensitivity Analysis to Control the Far-Wake Unsteadiness Behind Turbines. *Energies* **2017**, *10*, 1599.
13. Frisch, U. *Turbulence*; Cambridge University Press: Cambridge, UK, 1995.
14. Pope, S.B. *Turbulent Flows*; Cambridge University Press: Cambridge, UK, 2000.
15. Mikkelsen, R. Actuator Disc Methods Applied to Wind Turbines. Ph.D. Thesis, Technical University of Denmark, Lyngby, Denmark, 2003.

16. Calaf, M.; Meneveau, C.; Meyers, J. Large eddy simulation study of fully developed wind-turbine array boundary layers. *Phys. Fluids* **2010**, *22*, 015110, doi:10.1063/1.3291077.
17. Lu, H.; Porte-Agel, F. Large-eddy simulation of a very large wind farm in a stable atmospheric boundary layer. *Phys. Fluids* **2011**, *23*, 065101, doi:10.1063/1.3589857.
18. Wu, Y.T.; Porte-Agel, F. Large-Eddy Simulation of Wind-Turbine Wakes: Evaluation of Turbine Parametrisations. *Bound.-Layer Meteorol.* **2011**, *138*, 345–366.
19. Porté-Agel, F.; Wu, Y.T.; Lu, H.; Conzemius, R.J. Large-eddy simulation of atmospheric boundary layer flow through wind turbines and wind farms. *J. Wind Eng. Ind. Aerodyn.* **2011**, *99*, 154–168.
20. Goit, J.P.; Meyers, J. Analysis of turbulent flow properties and energy fluxes in optimally controlled wind-farm boundary layers. *J. Phys. Conf. Ser.* **2014**, *524*, 012178, doi:10.1088/1742-6596/524/1/012178.
21. VerHulst, C.; Meneveau, C. Large eddy simulation study of the kinetic energy entrainment by energetic turbulent flow structures in large wind farms. *Phys. Fluids* **2014**, *26*, 025113, doi:10.1063/1.4865755.
22. Witha, B.; Steinfeld, G.; Heinemann, D. High-resolution offshore wake simulations with the LES model PALM. In *Wind Energy-Impact Turbul*; Springer: Berlin/Heidelberg, Germany, 2014.
23. Dörenkämper, M.; Witha, B.; Steinfeld, G.; Heinemann, D.; Kühn, M. The impact of stable atmospheric boundary layers on wind-turbine wakes within offshore wind farms. *J. Wind Eng. Ind. Aerodyn.* **2015**, *144*, 146–153.
24. Stevens, R.J.A.M.; Gayme, D.F.; Meneveau, C. Effects of turbine spacing on the power output of extended wind-farms. *Wind Energy* **2016**, *19*, 359–370.
25. Jensen, N.O. *A Note on Wind Generator Interaction*; Risø National Laboratory: Roskilde, Denmark, 1983.
26. Frandsen, S.; Barthelmie, R.; Pryor, S.; Rathmann, O.; Larsen, S.; Hojstrup, J.; Thogersen, M. Analytical modelling of wind speed deficit in large offshore wind farms. *Wind Energy* **2006**, *9*, 39–53.
27. Quarton, D.; Ainslie, J. Turbulence in wind turbine wakes. *Wind Eng.* **1990**, *14*, 15–23.
28. Larsen, G.C.; Madsen Aagaard, H.; Bingöl, F.; Mann, J.; Ott, S.; Sørensen, J.N.; Okulov, V.; Troldborg, N.; Nielsen, N.M.; Thomsen, K. *Dynamic Wake Meandering Modeling*; Risø-R 1607; Risø National Laboratory: Roskilde, Denmark, 2007.
29. Larsen, G.C.; Madsen, H.A.; Thomsen, K.; Larsen, T.J. Wake meandering: A pragmatic approach. *Wind Energy* **2008**, *11*, 377–395.
30. Madsen, H.A.; Larsen, G.C.; Larsen, T.J.; Troldborg, N.; Mikkelsen, R. Calibration and validation of the dynamic wake meandering model for implementation in an aeroelastic code. *J. Sol. Energy Eng.* **2010**, *132*, 041014, doi;10.1115/1.4002555.
31. Keck, R.E.; Maré, M.; Churchfield, M.J.; Lee, S.; Larsen, G.; Madsen, H.A. Two improvements to the dynamic wake meandering model: including the effects of atmospheric shear on wake turbulence and incorporating turbulence build-up in a row of wind turbines. *Wind Energy* **2015**, *18*, 111–132.
32. Larsen, T.J.; Madsen, H.A.; Larsen, G.C.; Hansen, K.S. Validation of the dynamic wake meander model for loads and power production in the Egmond aan Zee wind farm. *Wind Energy* **2013**, *16*, 605–624.
33. Singh, A.; Howard, K.B.; Guala, M. On the homogenization of turbulent flow structures in the wake of a model wind turbine. *Phys. Fluids* **2014**, *26*, doi:10.1063/1.4863983.
34. Bastine, D.; Wächter, M.; Peinke, J.; Trabucchi, D.; Kühn, M. Characterizing Wake Turbulence with Staring Lidar Measurements. *J. Phys. Conf. Ser.* **2015**, *625*, 012006, doi:10.1088/1742-6596/625/1/012006.
35. Andersen, S.J.; Sørensen, J.N.; Mikkelsen, R. Reduced order model of the inherent turbulence of wind turbine wakes inside an infinitely long row of turbines. *J. Phys. Conf. Ser.* **2014**, *555*, 012005, doi:10.1088/1742-6596/555/1/012005.
36. Andersen, S.J.; Sorensen, J.N.; Mikkelsen, R. Simulation of the inherent turbulence and wake interaction inside an infinitely long row of wind turbines. *J. Turbul.* **2013**, *14*, 1–24.
37. Bastine, D.; Witha, B.; Wächter, M.; Peinke, J. POD Analysis of a Wind Turbine Wake in a Turbulent Atmospheric Boundary Layer. *J. Phys. Conf. Ser.* **2014**, *524*, 012153, doi:10.1088/1742-6596/524/1/012153.
38. Bastine, D.; Witha, B.; Wächter, M.; Peinke, J. Towards a Simplified DynamicWake Model Using POD Analysis. *Energies* **2015**, *8*, 895–920.
39. Hamilton, N.; Tutkun, M.; Cal, R.B. Wind turbine boundary layer arrays for Cartesian and staggered configurations: Part II, low-dimensional representations via the proper orthogonal decomposition. *Wind Energy* **2015**, *18*, 297–315.

40. Hamilton, N.; Tutkun, M.; Cal, R.B. Low-order representations of the canonical wind turbine array boundary layer via double proper orthogonal decomposition. *Phys. Fluids* **2016**, *28*, 025103, doi:10.1063/1.4940659.
41. Iungo, G.V.; Santoni-Ortiz, C.; Abkar, M.; Porté-Agel, F.; Rotea, M.A.; Leonardi, S. Data-driven Reduced Order Model for prediction of wind turbine wakes. *J. Phys. Conf. Ser.* **2015**, *625*, 012009, doi:10.1088/1742-6596/625/1/012009.
42. Sarmast, S.; Dadfar, R.; Mikkelsen, R.F.; Schlatter, P.; Ivanell, S.; Sorensen, J.N.; Henningson, D.S. Mutual inductance instability of the tip vortices behind a wind turbine. *J. Fluid Mech.* **2014**, *755*, 705–731.
43. Debnath, M.; Santoni, C.; Leonardi, S.; Iungo, G.V. Towards reduced order modelling for predicting the dynamics of coherent vorticity structures within wind turbine wakes. *Philos. Trans. A Math. Phys. Eng. Sci.* **2017**, *375*, pii: 20160108, doi:10.1098/rsta.2016.0108.
44. Ali, N.; Cortina, G.; Hamilton, N.; Calaf, M.; Cal, R.B. Turbulence characteristics of a thermally stratified wind turbine array boundary layer via proper orthogonal decomposition. *J. Fluid Mech.* **2017**, *828*, 175–195.
45. Araya, D.B.; Colonius, T.; Dabiri, J.O. Transition to bluff-body dynamics in the wake of vertical-axis wind turbines. *J. Fluid Mech.* **2017**, *813*, 346–381.
46. Tabib, M.; Siddiqui, M.S.; Fonn, E.; Rasheed, A.; Kvamsdal, T. Near wake region of an industrial scale wind turbine: comparing LES-ALM with LES-SMI simulations using data mining (POD). *J. Phys. Conf. Ser.* **2017**, *854*, 012044, doi:10.1088/1742-6596/854/1/012044.
47. Hamilton, N.; Tutkun, M.; Cal, R.B. Anisotropic character of low-order turbulent flow descriptions through the proper orthogonal decomposition. *Phys. Rev. Fluids* **2017**, *2*, doi:10.1103/PhysRevFluids.2.014601.
48. Berkooz, G.; Holmes, P.; Lumley, J.L. The Proper Orthogonal Decomposition In the Analysis of Turbulent Flows. *Ann. Rev. Fluid Mech.* **1993**, *25*, 539–575.
49. Cordier, L.; Noack, B.R.; Tissot, G.; Lehnasch, G.; Delville, J.; Balajewicz, M.; Daviller, G.; Niven, R.K. Identification strategies for model-based control. *Exp. Fluids* **2013**, *54*, 1580, doi:10.1007/s00348-013-1580-9.
50. Schmid, P.J. Dynamic mode decomposition of numerical and experimental data. *J. Fluid Mech.* **2010**, *656*, 5–28.
51. Jovanović, M.R.; Schmid, P.J.; Nichols, J.W. Sparsity-promoting dynamic mode decomposition. *Phys. Fluids* **2014**, *26*, 024103, doi:10.1063/1.4863670.
52. Le Clainche, S.; Vega, J.M. Higher order dynamic mode decomposition to identify and extrapolate flow patterns. *Phys. Fluids* **2017**, *29*, 084102, doi:10.1063/1.4997206.
53. Kou, J.; Le Clainche, S.; Zhang, W. A reduced-order model for compressible flows with buffeting condition using higher order dynamic mode decomposition with a mode selection criterion. *Phys. Fluids* **2018**, *30*, 016103, doi:10.1063/1.4999699.
54. Andersen, S.J. Simulation and Prediction of Wakes and Wake Interaction in Wind Farms. Ph.D. Thesis, Technical University of Denmark, Lyngby, Denmark, 2014.
55. Iungo, G.V.; Wu, Y.T.; Porte-Agel, F. Field Measurements of Wind Turbine Wakes with Lidars. *J. Atmos. Ocean. Technol.* **2013**, *30*, 274–287.
56. Witha, B.; Steinfeld, G.; Heinemann, D. Advanced turbine parameterizations in offshore LES wake simulations. In Proceedings of the 6th Intenational Symposium on Computational Wind Engineering, Hamburg, Germany, 8–13 June 2014.
57. Raasch, S.; Schroter, M. PALM—A large-eddy simulation model performing on massively parallel computers. *Meteorol. Z.* **2001**, *10*, 363–372.
58. Maronga, B.; Gryschka, M.; Heinze, R.; Hoffmann, F.; Kanani-Sühring, F.; Keck, M.; Ketelsen, K.; Letzel, M.O.; Sühring, M.; Raasch, S. The Parallelized Large-Eddy Simulation Model (PALM) version 4.0 for atmospheric and oceanic flows: Model formulation, recent developments, and future perspectives. *Geosci. Model Dev.* **2015**, *8*, 2515–2551.
59. Deardorff, J.W. Stratocumulus-capped mixed layers derived from a three-dimensional model. *Bound.-Layer Meteorol.* **1980**, *18*, 495–527.
60. Vollmer, L.; Steinfeld, G.; Heinemann, D.; Kühn, M. Estimating the wake deflection downstream of a wind turbine in different atmospheric stabilities: An LES study. *Wind Energy Sci. Discuss.* **2016**, *1*, 129–141, doi:10.5194/wes-1-129-2016.
61. Wang, T. A brief review on wind turbine aerodynamics. *Theor. Appl. Mech. Lett.* **2012**, *2*, 062001, doi:10.1063/2.1206201.

62. Jonkman, J.M.; Butterfield, S.; Musial, W.; Scott, G. *Definition of a 5-MW Reference Wind Turbine for Offshore System Development*; Technical Report NREL/TP-500-38060; National Renewable Energy Laboratory: Golden, CO, USA, 2009.
63. Serra, J. *Image Analysis and Mathematical Morphology, V. 1*; Academic Press: New York, NY, USA, 1982.
64. Risken, H. *Fokker-Planck Equation*; Springer: New York, NY, USA, 1984.
65. Gardiner, C.W. *Handbook of Stochastic Methods*; Springer: Berlin, Germany, 1985; Volume 3.
66. Friedrich, R.; Peinke, J.; Sahimi, M.; Reza Rahimi Tabar, M. Approaching complexity by stochastic methods: From biological systems to turbulence. *Phys. Rep.* **2011**, *506*, 87–162.
67. Kantz, H.; Schreiber, T. *Nonlinear Time Series Analysis*; Cambridge University Press: Cambridge, UK, 2004; Volume 7.
68. Jonkman, J.M.; Buhl, M.L., Jr. *FAST User's Guide, NREL/EL-500-29798*; Technical Report; National Renewable Energy Laboratory: Golden, Colorado, USA, 2005.
69. Laino, D. *NWTC Design Code AeroDyn v12.58*; Technical Report; National Renewable Energy Laboratory: Golden, CO, USA, 2005.
70. Burton, T.; Sharpe, D.; Jenkins, N.; Bossanyi, E. *Wind Energy Handbook*; Wiley: New York, NY, USA, 2011.
71. Nieslony, A. *Rainflow Counting Algorithm (Version 1.2)*; Mathworks, Matlab Central: Natick, CA, USA, 2010.
72. ASTM E1049-85. *Standard Practices for Cycle Counting in Fatigue Analysis*; ASTM: West Conshohocken, PA, USA, 1994.
73. Saranyasoontorn, K.; Manuel, L. Low-dimensional representations of inflow turbulence and wind turbine response using proper orthogonal decomposition. *J. Sol. Energy Eng.* **2005**, *127*, 553–562.
74. Saranyasoontorn, K.; Manuel, L. Symmetry considerations when using proper orthogonal decomposition for predicting wind turbine yaw loads. *J. Sol. Energy Eng.-Trans.* **2006**, *128*, 574–579.
75. Mann, J. Wind field simulation. *Probab. Eng. Mech.* **1998**, *13*, 269–282.
76. Kleinhans, D. Stochastische Modellierung Komplexer Systeme—Von den Theoretischen Grundlagen zur Simulation Atmosphärischer Windfelder. Ph.D. Thesis, University of Münster, Münster, Germany, 2008.
77. Beck, H.; Davide, T.; Andreas, R.; vanDooren, M.; Kühn, M. Volumetric wind field measurements of wind turbine wakes with long-range lidars. In Proceedings of the EWEA Conference, Paris, France, 17–20 November 2015.
78. Barthelmie, R.J.; Doubrawa, P.; Wang, H.; Pryor, S.C. Defining wake characteristics from scanning and vertical full-scale lidar measurements. *J. Phys. Conf. Ser.* **2016**, *753*, 032034, doi:88/1742-6596/753/3/032034.
79. Chamorro, L.P.; Guala, M.; Arndt, R.E.A.; Sotiropoulos, F. On the evolution of turbulent scales in the wake of a wind turbine model. *J. Turbul.* **2012**, *13*, doi:10.1080/14685248.2012.697169.
80. Melius, M.S.; Tutkun, M.; Cal, R.B. Identification of Markov process within a wind turbine array boundary layer. *J. Renew. Sustain. Energy* **2014**, *6*, 023121, doi:10.1063/1.4869566.
81. Melius, M.S.; Tutkun, M.; Cal, R.B. Solution of the Fokker–Planck equation in a wind turbine array boundary layer. *Phys. D Nonlinear Phenom.* **2014**, *280*, 14–21.